Politecnico di Torino

Renewable Energy Systems
A.a. 2024/2025
Sessione di Laurea marzo 2025

Electrochemical nitrate reduction for green ammonia production: assessing the impact of real water composition for energy carrier applications

Supervisors:
Prof. Federico BELLA
Dr. Sara GARCIA BALLESTEROS

Candidate:
Lapo MASTRANDREA

Abstract

Ammonia (NH_3) has historically been an indispensable chemical, mainly as fertilizer. Recently, it has gained attention as a carbon-free energy carrier. Global ammonia production is dominated by the Haber-Bosch process, which is energy-intensive and generates significant CO_2 emissions. To keep global warming below 1.5 °C, as called for in the Paris Agreement, emissions need to be reduced by 45% by 2030 and reach net zero by 2050. As a result, developing a sustainable and efficient pathway for NH_3 synthesis is urgent. On the other hand, nitrates pollution in water bodies is a growing global concern. Nitrogen is a crucial element for life, but the intensification of human activities in agriculture leads to water contamination and a decline in water quality. When nitrate concentrations exceed a certain threshold, they can be harmful to human health. The electrocatalytic nitrate reduction reaction (NO_3RR) offers a pathway to achieve both ammonia production and water denitrification. This work aims to demonstrate the feasibility of ammonia production from electrocatalytic reduction of nitrates contained in real wastewater. For that purpose, the influence of various elements commonly found in real waters on NO_3RR was first evaluated. Then a simulated brackish water reverse osmosis brine, representative of real conditions, was used as the electrolyte in the NO_3RR process. The efficiency was markedly lower when real brackish water was used as the electrolyte, highlighting the challenges associated with complex water matrices.

Table of Contents

List of Figures

List of tables

Chapter 1

1. Introduction

1.1 Nitrates pollution in water bodies

Nitrogen is a crucial nutrient essential for plant and crops grow, however, high concentrations can be harmful to both human health and the environment. One of the main sources of nitrogen pollution in Europe is agricultural runoff, where nitrates and organic nitrogen compounds from fertilizers and manure leach into groundwater and reach surface water through runoff from agricultural fields. Due to their high-water solubility, these compounds are very susceptible to contamination, making nitrogen leakage a serious concern. In rivers, lakes and marine ecosystems, nitrogen and other nutrients stimulate algae growth. While at moderate levels, algal growth is beneficial as food source for aquatic organisms, excessive nitrogen concentration can cause algal blooms, affecting the natural ecosystem and leading to the depletion of oxygen in the water. This phenomenon, known as eutrophication, negatively impacts biodiversity by increasing water turbidity, which reduces the light penetration to deeper layers of the ecosystem. As a result, submerged vegetation is unable to photosynthesize and ultimately dies.

Beyond its environmental consequences, excessive nitrates levels cause serious human health risk. The ingestion of water with excessive nitrate concentration can disable oxygen carriers, causing the methemoglobinemia. As a result, the World Health Organization (WHO) and the Council of European Union have set a limit on NO_3^- concentration in drinking water of 50 mg L^{-1}. [1] Additionally, the Food and Agriculture Organization of the United Nations (FAO) has set a limit on NO_3^- concentration in water for irrigation of 22 mg L^{-1}. [2]

1.1.1 Human influence on the nitrogen cycle

Nitrogen is the most abundant element on Earth, making up 78.1% of the atmospheric volume. Despite this, it is relatively scarce in the Earth's crust due to the volatility of nitrogen compounds, which limits their presence in solid geological deposits. [3] Nitrogen is indispensable for plant health, as it enables the production of amino acids, the building blocks of proteins. These proteins, in turn, promote robust plant growth. The efficient use of nitrogen is responsible for an increase in root length, diameter and biomass content in the roots. However, excess of nitrogen can be toxic to plants and detrimental to the environment. In its molecular form (N_2), nitrogen is not available to plants; therefore, it must be fixed into an accessible form so plants can absorb and use it. Fixation refers to the conversion into reactive nitrogen (Nr), which includes inorganic reduced forms (NH_3 and NH_4^+), inorganic oxidized forms (NO, NO_2, HNO_3, N_2O and NO_3^-) and organic compounds (urea, amines and proteins). This process can occur biologically through nitrogen-fixing bacteria or anthropogenically via the Haber-Bosch process. The nitrogen cycle (Figure 1) is the biogeochemical cycle that describes the movement and conversion of nitrogen through different forms in the environment, including the atmosphere, soil, water and living organisms. Human activities such as fossil fuel consumption, intensive fertilizers use and nitrogen release in wastewater have drastically altered the nitrogen cycle. While most of the human-driven nitrogen inputs occur on a local scale, these activities have not only increased the availability but also intensified its global transport through air and water. As a result, long-term environmental consequences extend across large region of the Earth. The human impact on the nitrogen cycle is manifested in the following phenomena: [4]

- Increase of global concentrations of nitrous oxide (N_2O), a potent greenhouse gas, and of local concentrations of nitric oxide (NO)
- Depletion of soil nutrients such as calcium and potassium
- Acidification of soils and waters
- Increased nitrogen transport by rivers

- Water pollution

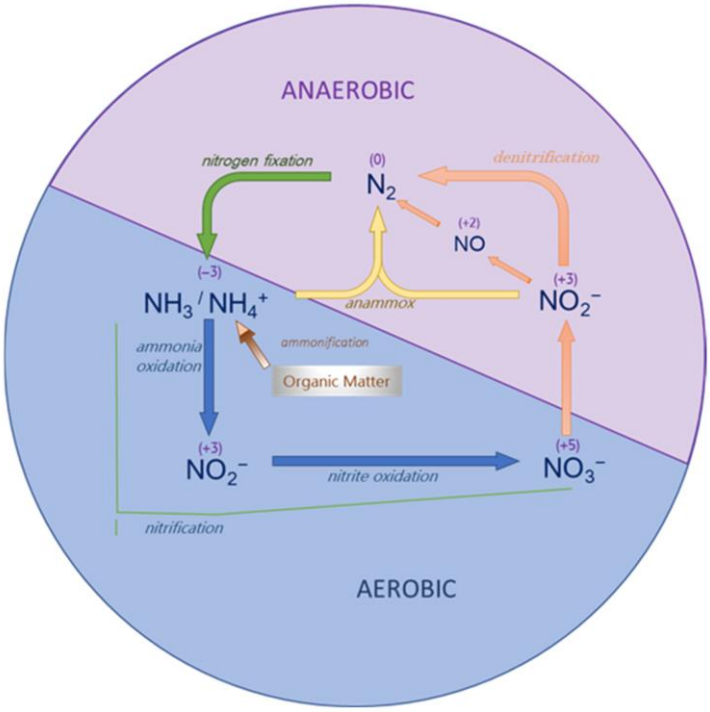

Figure 1: the biological nitrogen cycle [5]

Although natural sources contribute to nitrate pollution in water, the main contamination is attributed to anthropogenic activities. Human actions have double the nitrogen input rate into the global nitrogen cycle, increasing it by 100%. [5] The abuse of N-based fertilizers in agriculture is the major source of NO_3^- contamination in waterbodies. Fertilizers are often applied in quantities above the nutritional needs of the crops, resulting in only partial assimilation by plants. The excess nitrogen leach into groundwater, contributing to widespread pollution. Additionally, the development of high-density populated urban centres and intensive livestock farming are significant contributors to nitrate pollution in wastewater. Livestock waste contains nitrogen in different forms, which are converted into NO_3^- by microbial actions, further polluting surrounding waterbodies. Lastly, industrial

processes (mostly chemical industries) also contribute to NO_3^- pollution in the environment, mostly due to inadequate waste management.

1.1.2Health risks

In soil and water, microorganisms convert nitrates into nitrites. Excessive nitrite consumption can interfere with the oxygen transportation in blood causing methemoglobinemia, also known as *blue baby syndrome*.

In the oral cavity, a part of the consumed nitrate is reduced to nitrite by nitrate-reducing bacteria. In infants under six months, nitrates oxidise haemoglobin into methaemoglobin, which has a reduced capacity to transport oxygen. This lack of oxygen causes cyanosis, leading to a bluish discoloration of the skin, particularly around the eyes and mouth. Additionally, excessive nitrate intake has also been linked to cancer risk. Nitrate is a precursor in the formation of N-nitroso compounds (NOC), and most of them are known carcinogens. [6]

1.1.3 Nitrates directives

Several directives regulate nitrogen losses to the environment. The Groundwater Directive and the Drinking Water Directive from WHO have set the maximum allowable concentration of nitrate at 50 mg L^{-1} in EU. ([7], [8]) For the United States, the maximum contaminant level (MCL) for nitrate in public drinking water is 10 mg L^{-1} as nitrate-nitrogen (NO_3^--N), which is approximately equivalent to the limit set by WHO (50 mg L^{-1} as NO_3^- or 11.3 mg L^{-1} as NO_3^--N). [6] The Nitrates Directive, issued in 1991, requires EU members to monitor the quality of waters and to identify areas that drain into polluted waters or at risk of pollution. The aim of the directive is to protect water quality across Europe by preventing nitrates pollution from agricultural sources and by promoting sustainable farming practices. The directive designates areas affected by agricultural eutrophication or at risk of exceeding 50 mg L^{-1} as Nitrate Vulnerable Zones (NVZs), where stricter regulations apply to mitigate contamination.

Every four years, EU members are required to report on: [9]

- nitrate concentration in groundwaters and surface waters
- eutrophication of surface waters
- assessment of the impact of action programs on water quality and agricultural practices
- revision of NVZs and action programs
- estimation of future trends in water quality

Despite the implementation of the directive, the average nitrate concentration in EU groundwaters did not change significantly, oscillating around 21 mg L^{-1} (Figure 2). Furthermore, an increase of groundwater monitoring stations exceeding the limit concentration of 50 mg L^{-1} was observed from the Nitrate Directive reporting data between the period 2012-2015 and 2016-2019, going from 13.2% to 14.1%. [10]

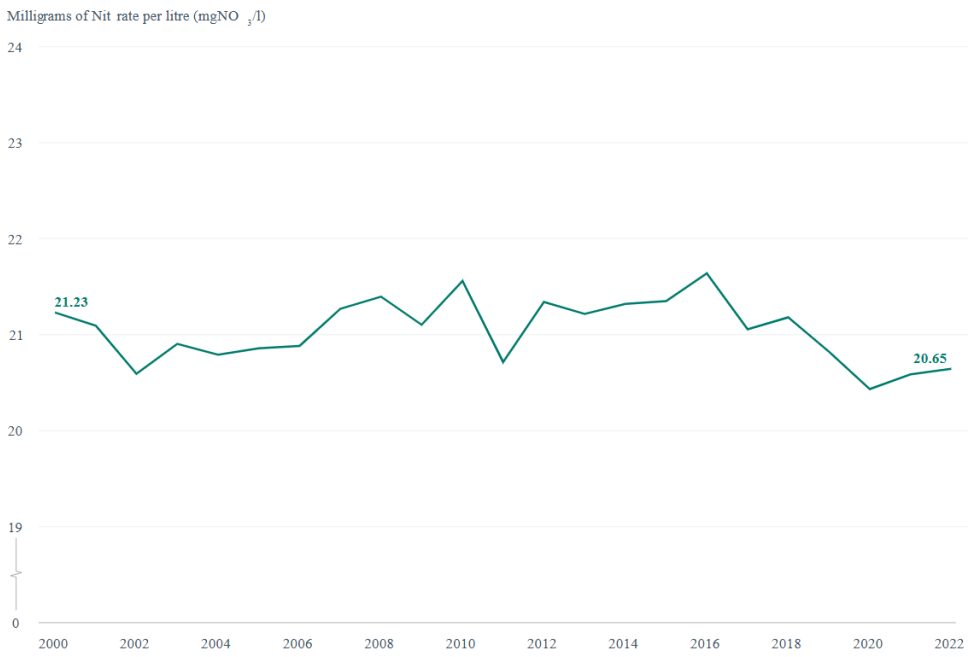

Figure 2: groundwater nitrate concentration in EU, 2000-2022 [11]

Considering a typical Nitrate Directive report, nitrate concentration in groundwater is divided into four classes:

- Class 1 → < 25 mg L^{-1}
- Class 2 → 25-40 mg L^{-1}
- Class 3 → 40-50 mg L^{-1}
- Class 4 → ≥ 50 mg L^{-1}

During the period 2016-2019, all 27 EU members had some groundwaters with nitrate concentrations above the limit of 50 mg L^{-1}. During this period, Malta was the country with the highest percentage of groundwater monitoring stations exceeding 50 mg L^{-1}, followed by Germany and Spain. These three, together with Belgium, Cyprus, Luxemburg and Portugal, were the only countries with a percentage of Class 4 groundwaters higher than 15%. On the other hand, Croatia, Finland, Hungary, Ireland, Latvia, Poland and Sweden were the only countries with a percentage of Class 1 groundwaters higher than 80%. Italy was between these two extreme situations, with a percentage of Class 1 and Class 4 groundwaters around 70% and 10%, respectively (Figure 3).

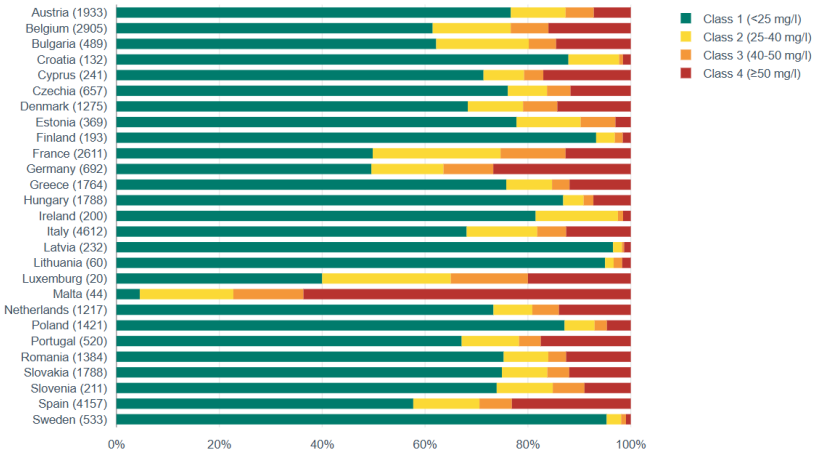

Figure 3: Nitrate concentrations in groundwater monitoring stations, 2016-2019 [10]

Considering the surface waters during the period 2016-2019, the following map shows the fractions of surface waters monitoring stations with concentration above 10 mg L^{-1} (Figure 4). During this period, the countries with the highest number of surface waters monitoring stations exceeding 10 mg L^{-1} were France, Germany and United Kingdom, with a variable percentage between 33.8% and 93%. On the other hand, the countries with the lowest percentage (< 3%) were Sweden, Poland, Finland, Portugal and Greece. In the case of Italy, the percentage was between 19.4% and 33.8%.

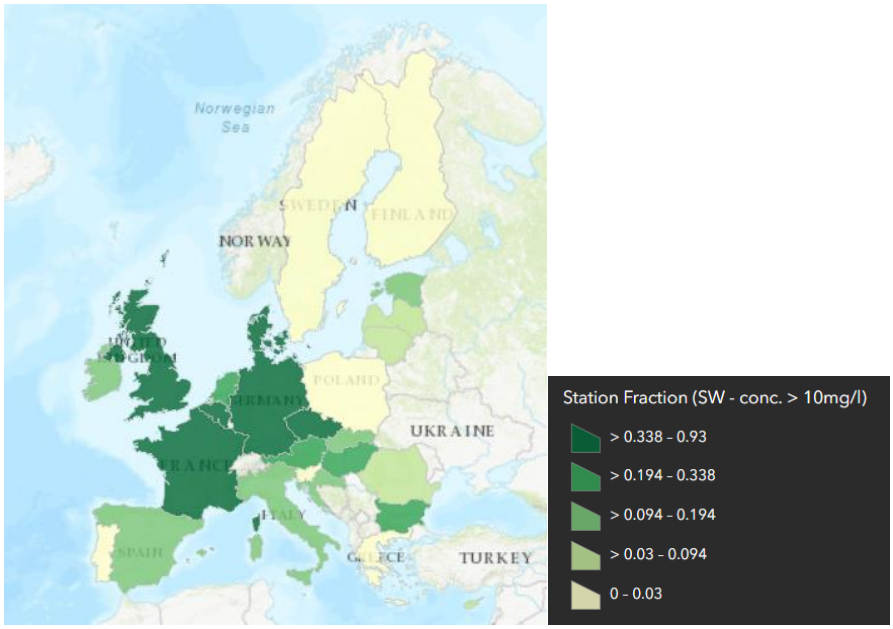

Figure 4: Nitrate concentrations in surface water monitoring stations, 2016-2019 [9]

1.1.4 Nitrate removal technologies

At the moment, two types of denitrification technologies exist: separation-based technologies, where the nitrates are removed from the water is concentrated in a waste product called brine, and transformation-based technologies where the nitrate is converted into another harmless chemical compound. Separation-based

technologies are the most used but are affected by high costs. Furthermore, the nitrate is not converted into a harmless compound but just concentrated in a brine. Among separation-based technologies, ion exchange is one of the most promising ones. It utilizes a selective resin, which is a synthetic material with positively charged sites that attract and hold negatively charged ions like nitrate. Typically, chloride ions (Cl^-) are used. When contaminated water passes through the resin, the nitrate ions are exchanged with chloride ions. After the resin has absorbed a certain amount of nitrate, it becomes saturated and needs to be regenerated. While ion exchange is often preferred for selective nitrate removal, reverse osmosis is also effective for general purification. Reverse osmosis systems utilize a semi-permeable membrane, with pore size in the order of 1 nm, to filter water. Water is pushed under pressure through the membrane, and the pores block the passage of large particles like nitrate ions (Figure 5). Reverse osmosis allows to obtain a high-quality water after the treatment, and for this reason is the most used technique in the world for water desalination processes. However, it requires a high energy demand, around 1.8-2.0 kWh m^{-3} [12], and it generates a waste containing high concentrations of nitrate, among others.

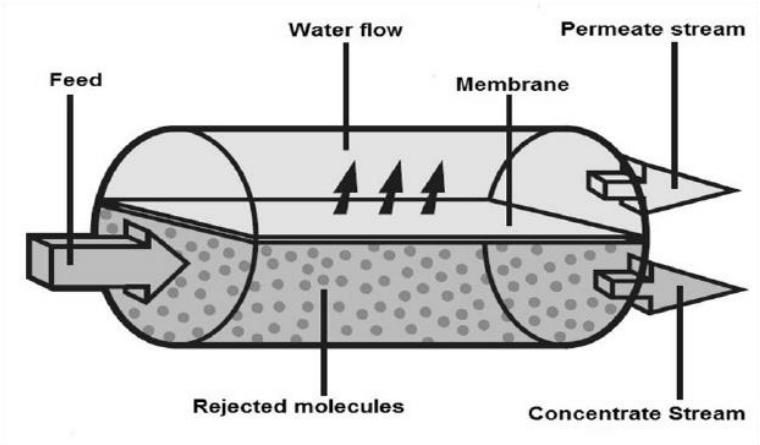

Figure 5: schematic diagram of reverse osmosis process [13]

In transformation-based technologies, nitrates are usually converted into dinitrogen. The reduction process can be performed by microorganisms or by electrochemical reactions. Biological denitrification is a process driven by bacteria under anaerobic conditions. Bacteria, such as Pseudonomas or Paracoccus, reduce nitrate through a series of enzymatic reactions. Nitrate is first reduced to nitrite, and then further reduced to nitrogen gas, which is released into the atmosphere. Bacteria need a carbon source and an electron donor substance to carry out the process, so pre-treatment of the water is required. Denitrification efficiencies of 95-100% are obtained using ethanol as electron donor in waterbodies with nitrate concentration > 250 mg L^{-1}. [14] Although biological denitrification is a highly efficient process, it has several drawbacks, such as a decrease in the denitrification rate when the temperature drops, which makes necessary additional treatment of the water.
Electrochemical denitrification is a relatively newer approach for removing nitrates from water using electrochemical reactions. In this process, an electrical current is applied to reduce nitrate ions (NO_3^-) to nitrogen gas. The electrochemical cell, consisting of an anode and a cathode, can be a single-chamber cell (SCC) or dual-chamber cell (DCC). The difference is the presence of a cation exchange membrane in the DCC, which prevents the re-oxidation of the nitrates at the anode (Figure 6). The advantages of electrochemical with respect to biological denitrification are:

- Faster process speed
- No microbial dependency
- No organic carbon required
- Scalability
- Continuous operation
- Fewer chemicals required and sludge generated

While electrochemical denitrification offers significant advantages, it also faces challenges like energy consumption, electrode fouling and high capital costs.

However, with continued research and development, these systems are becoming increasingly viable for addressing nitrate contamination in water systems.

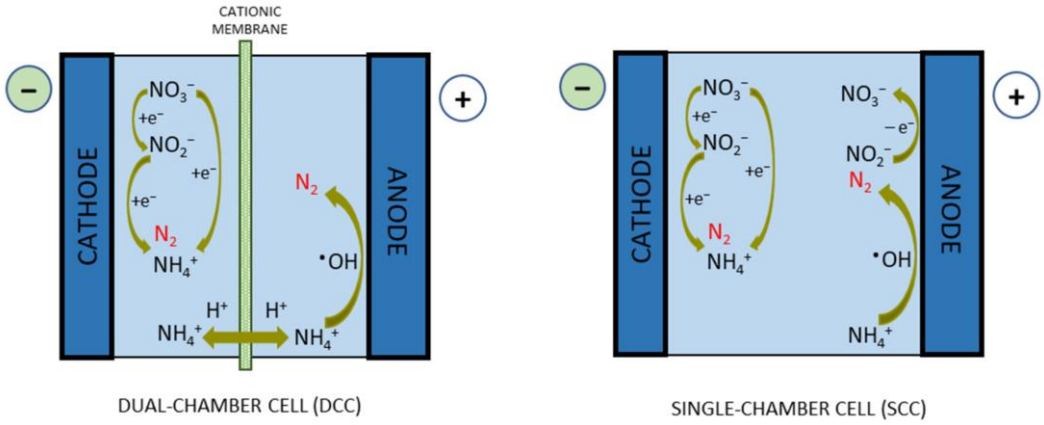

Figure 6: electrochemical reduction of nitrate ions in DCC and SCC [5]

1.2 Ammonia production processes

Ammonia is critical in the manufacturing of fertilizers and is one of the largest-volume synthetic chemicals produced in the world. About 70% of the produced ammonia is used for fertilizers, while the remaining 30% is used for industrial applications such as plastics, explosives and synthetic fibres. [15] Without the crop-yield made possible by ammonia-based fertilizers and chemicals, the global population would be at least 2 to 3 billion less that it is today. [16] The dominant ammonia production technology is the Haber-Bosch process, invented in 1904. It requires very high temperature (≈500 °C) as well as very high pressure (150-300 bar) [17], making it highly energy-intensive and reliant on fossil fuels, which leads to significant CO_2 emissions. Consequently, emerging technologies, such as electrocatalytic processes, are gaining interest as sustainable alternatives to reduce global emissions.

1.2.1 The Haber-Bosch process

In 1906, Haber developed a process for producing commercial quantities of ammonia, by passing a mixture of N_2 and H_2 across an osmium catalyst with high temperature and pressure. Haber process included a recycle system, to increase the ammonia production from the makeup gases. In 1910, Bosch developed the Haber process by promoting an iron catalyst for the reaction and designing a system configuration that could withstand the high temperatures and pressure. The first commercial ammonia production plant based on Haber-Bosch process was built in Oppau (Germany) in 1913, with a production capacity of 30 mt day^{-1}. [18]

In the Haber-Bosch process, atmospheric nitrogen (N_2) reacts with hydrogen (H_2) to form ammonia (NH_3). The reaction is the following:

$$N_2 + 3H_2 \leftrightarrow 2NH_3 \qquad \Delta H^0_{298K} = -92.28\ kJ\ mol^{-1} \qquad (1.1)$$

The reaction is thermodynamically favourable at room temperature, but the kinetics are very slow. At high temperature, instead, the equilibrium is shifted towards the reactants. A temperature of around 500 °C is a reasonable compromise to produce high proportion of ammonia in the equilibrium mixture in a very short time. Increasing the pressure brings the molecules close together, improving the kinetics of the reaction. However, dealing with very high pressures is expensive since stronger pipes and containment vessels are needed, increasing the capital costs of the plant. A pressure of around 200 bar is a good compromise between the price of the ammonia produced and the capital costs of the plant. [19]

Hydrogen required for ammonia synthesis is usually obtained from gasification of carbon-containing materials, such as natural gas, coal and biomass. Steam methane reforming (SMR) is the most common method for producing hydrogen from natural gas. The reaction is represented by this equilibrium:

$$CH_4 + H_2O \leftrightarrow CO + 3H_2 \qquad \Delta H = 206\ kJ\ mol^{-1} \qquad (1.2)$$

The reaction is highly endothermic; therefore, a large amount of heat is required. Optimal operating conditions for SMR are 800-900 °C of temperature and 20-30 bar of pressure. [20]

Water gas shift reaction (WGSR) is also used to produce additional hydrogen from the reaction of the previously generated carbon monoxide (CO) with water:

$$CO + H_2O \leftrightarrow CO_2 + H_2 \qquad \Delta H = -41\ kJ\ mol^{-1} \qquad (1.3)$$

Carbon monoxide and carbon dioxide must be removed from the gas mixture by using gas scrubbing, because together with ammonia could form carbamates which could clog the pipelines. Before entering the reactor, the gas mixture is compressed by turbo compressors. The hydrogen-nitrogen mixture entering the reactor is preheated by the outgoing reaction mixture. While removing the ammonia from the system increases the reaction yield, this step is usually avoided since the temperature is too high. In practice, hot gases exiting the reaction vessel are cooled under high pressure, allowing the ammonia to condense and be removed as a liquid, while condensed nitrogen and hydrogen are recirculated back to the reaction vessel (Figure 7). Currently, ammonia synthesis by Haber-Bosch is the industrial process that emits the highest amount of carbon dioxide, with 1.6 ton of CO_2 released for every ton of produced ammonia. [21] The process is energy intensive, accounting for 1-2% of global energy consumption, 3% of global carbon emissions [22] and 3-5% of global natural gas consumption. [23] Carbon dioxide is a greenhouse gas and the environmental impact from its emission can affect food, water, water, sea level and weather patterns. So, the production of ammonia, designed to improve food yields, is having an indirectly negative impact on food and water supplies. For this reason, other sustainable ammonia production processes are being extensively explored. Ammonia produced via the standard Haber-Bosch process is called “grey ammonia”. An alternative to reduce CO_2 emissions is the production of the so called “green ammonia”. The main difference between the green and the grey ammonia, is that the former uses hydrogen produced by electrolysis of water using electricity

from renewable sources, while the latter uses hydrogen produced by steam reforming of natural gas. Green ammonia does not emit CO_2 during its production, and it can contribute to climate change mitigation. However, the production of green ammonia still requires high energy consumption due to the high temperatures and pressures needed for the Haber-Bosch process. To solve this problem, an even greener process, such as the electrochemical synthesis of ammonia, is needed.

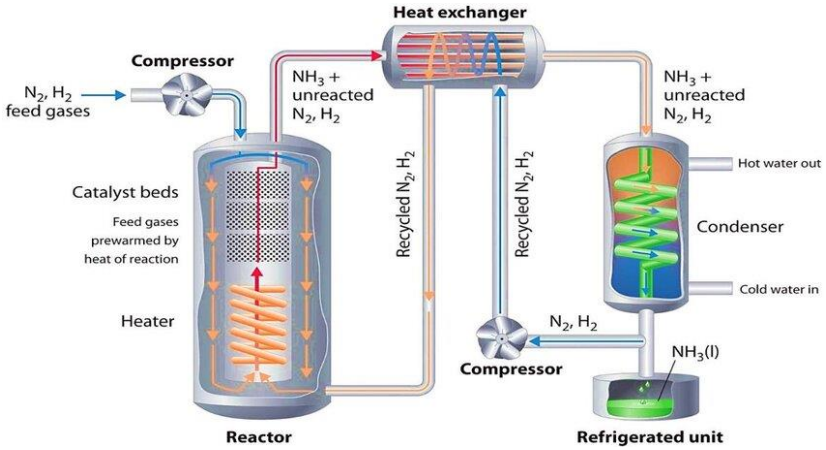

Figure 7: Schematic diagram of the Haber-Bosch process [24]

1.2.2 Electrochemical synthesis of ammonia

Unlike the Haber-Bosch process, electrochemical synthesis of ammonia has the advantages of mild operating conditions, zero emissions of carbon dioxide and the possibility for distributed ammonia production. There are three main ways of producing ammonia electrochemically:

- Electrocatalytic nitrogen reduction reaction (NRR)
- Lithium-mediated nitrogen reduction reaction (Li-NRR)
- Electrocatalytic nitrate or nitrite reduction reaction (NO_3RR and NO_2RR)

NRR faces different problems such as poor selectivity and low NH_3 yield, due to the low solubility of nitrogen gas in water (0.66 mmol/L), high dissociation energy

of the triple bond N≡N (945 kJ/mol), sluggish reaction kinetics and the competition with the hydrogen evolution reaction (HER). [25] The HER is an electrochemical reaction in which hydrogen gas (H_2) is produced by the reduction of protons (H^+) or water at the cathode.

In acidic electrolytes: [26]

$$N_2 + 6H^+ + 6e^- \rightarrow 2NH_3 \qquad E^0 = 0.148\,V\ vs\ RHE \tag{1.4}$$

$$2H^+ + 2e^- \rightarrow H_2 \qquad E^0 = 0\,V\ vs\ SHE \tag{1.5}$$

In basic electrolytes:

$$N_2 + 6H_2O + 6e^- \rightarrow 2NH_3 + 6OH^- \qquad E^0 = -0.736\,V\ vs\ SHE \tag{1.6}$$

$$2H_2O + 2e^- \rightarrow H_2 + 2OH^- \qquad E^0 = -0.828\,V\ vs\ SHE \tag{1.7}$$

The reduction potential (E^0) is a measure of the tendency of a chemical species to gain electrons and undergo reduction. It is usually measured in volts (V) and is typically referenced against a standard hydrogen electrode (SHE) or, in this case, reversible hydrogen electrode (RHE). The more positive the reduction potential, the greater the tendency of the substance to gain electrons and be reduced. The electrochemical NRR and HER both can occur from a thermodynamic point of view and their reduction potentials are very similar. However, NRR involves six electrons and six protons, while HER involves only two electrons. For this reason, HER is more kinetically preferred.

In the case of Li-NRR, the triple bond N≡N is broken during the reaction between N_2 and metallic Li, leading to higher Faradaic efficiency (FE).

NO_3RR faces the problem of sluggish reaction kinetics as it involves complicated eight-electron transfer pathways, as well as the competition with the HER. The reduction potentials of different nitrogen sources are the following: [27]

$$NO_3^- + 6H_2O + 8e^- \rightarrow NH_3 + 9OH^- \qquad E^0 = -0.12\,VvsRHE \qquad (1.8)$$

$$NO_2^- + 5H_2O + 6e^- \rightarrow NH_3 + 7OH^- \qquad E^0 = -0.17\,VvsRHE \qquad (1.9)$$

$$N_2 + 6H_2O + 6e^- \rightarrow 2NH_3 + 6OH^- \qquad E^0 = 0.09\,VvsRHE \qquad (1.10)$$

Comparing the reduction potentials, the NRR is thermodynamically the most favourable way to produce ammonia, but NO_2^- and NO_3^- have much lower N-O bond dissociation energy (204 kJ/mol) which promotes more favorable kinetics for that NO_3RR or NO_2RR. [25] In particular, NO_3^- is more stable than NO_2^- because of the high oxidation state. For these reasons, NO_3RR is the most developed electrochemical technology to produce ammonia.

1.2.3 Future scenarios

There are three possible future scenarios for ammonia production: the Stated Policies Scenario, where the industry follows current trends; the Sustainable Development Scenario, where the industry adopts policies required to align with the goals of the Paris Agreement; the Net Zero Emissions by 2050 Scenario, where the industry adopts policies required to reach net zero emissions globally by 2050. [15] To reach this goal, near-zero-emission technologies are emerging, including electrolysis and fossil fuel with carbon capture and storage (CCS). These technologies are usually much more expensive per tonne of ammonia produced than conventional ones, and so further development is needed. In the Sustainable Development Scenario, the share of near-zero-emission technologies reaches almost 70% of total production by 2050, up from less than 1% today. Natural gas-based production with the implement of CCS accounts for around 20% of total

production, while the share of electrolysis is more than 25%. In the Net Zero Emissions by 2050 Scenario, the share of near-zero emission technologies reaches almost 95% of total production by 2050. Natural gas-based production with the implement of CCS accounts for around 20% of total production, while the share of electrolysis is more than 40% (Figure 8).

However, these scenarios face different challenges: most near-zero-emission technologies are not yet available in the market at commercial scale, but are still in the development phase, and the Scenarios require a rapid deployment of these technologies to reach the goals by 2050.

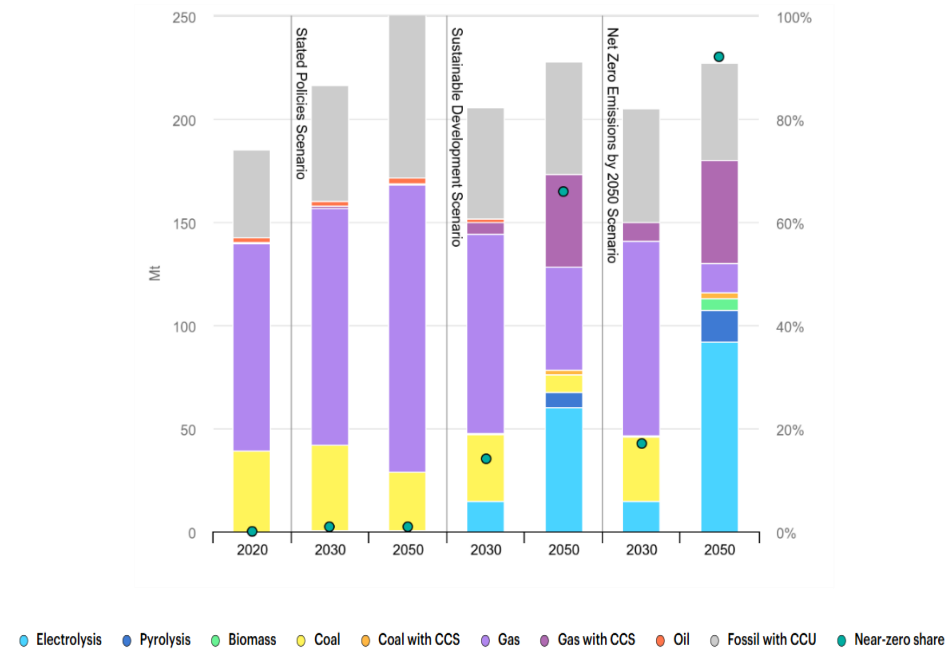

Figure 8: Global ammonia production by technology and scenario, 2020-2050 [15]

1.3 Ammonia as an energy carrier

Paris agreement has set long-term goals to guide all nations to the reduction of global greenhouse gas emissions and the promotion of renewable energy. One of the main problems of renewable energy is the intermittency. Wind and solar energy are intermittent, meaning that they do not generate electricity consistently all the time. Solar panels only work when the sun is shining, while wind turbines only produce power when the wind is blowing. To counter this problem, energy storage systems are needed to store energy generated during peak times for use it when the production is low. The global energy storage market in 2024 was estimated to be around 360 GWh. [28] Different forms of storage are currently available:

- Mechanical → pumped hydro energy storage (PHES), compressed air energy storage (CAES), liquid air energy storage (LAES), flywheel
- Electrical → capacitors, supercapacitors, superconducting magnetic energy storage (SMES)
- Electrochemical → batteries, flow batteries
- Thermal → low temperature (cryogenic), high temperature (heating systems)
- Chemical → hydrogen, methane, ammonia, methanol

For small amount of energy and short discharging times, the optimal solutions are capacitors, flywheel and batteries. For larger amounts of energy and longer discharging times, mechanical storage, such as CAES and PHES, is more suitable (Figure 9).

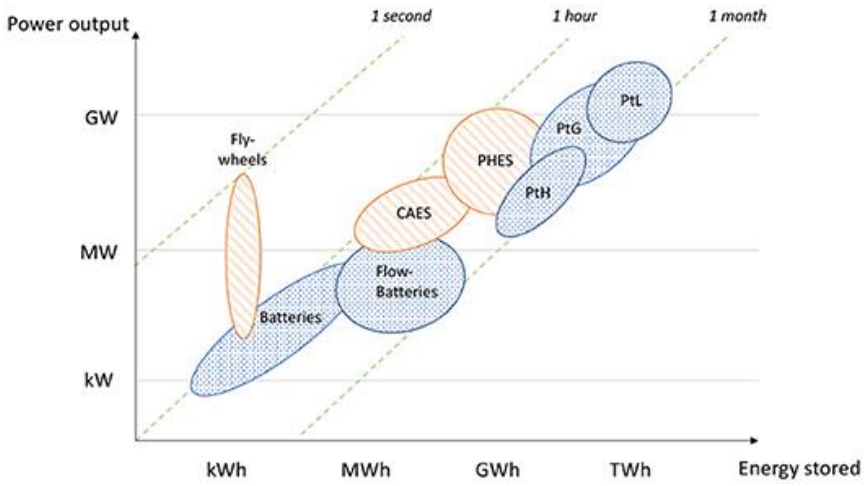

Figure 9: Power output vs Energy storage for different storage techniques [29]

1.3.1 Power-to-X

90% of the new energy storage deployments took place in the form of batteries between 2015 and 2024. Batteries are a crucial component of the recent growth in energy storage, particularly those based on lithium-ion. However, batteries face different challenges, such as a limited energy density, high environmental impact and a short lifespan. Therefore, for larger amounts of energy stored and longer-term storage (weeks), electricity can be stored through the production of fuels. This technique is called Power-to-X, and X represents the produced fuel. It can be a liquid (Power-to-Liquid, PtG), a gas (Power-to-Gas, PtG), or another chemical. To compare the suitability of different storage technologies, the economic costs of production, storage and transport, as well as the efficiency, need to be assessed. CAPEX is an economic indicator which refers to the capital expenditure made for the construction, upgrade, or expansion of the storage plant, while the Levelized Cost of Electricity (LCOE) is an economic indicator used to compare the cost of electricity generation from different energy sources. LCOE is obtained as the total cost of producing electricity from a specific energy source over its lifetime divided by the total amount of energy the plant is expected to generate over that time. The LCOES method is derived from LCOE, but accounts only for the storage system. Battery is the storage technology with the highest efficiency, but the high CAPEX

limits its applications. Mechanical storage (CAES and PHES) presents good efficiency and lower costs with respect to batteries. For this reason, mechanical storage is worldwide the most used technology. Power-to-X technology has the lowest LCOES despite much lower efficiency, demonstrating that it is competitive especially when huge quantities are to be stored (Table 1).

	Pumped hydro	CAES	Li-ion batteries	Flow batteries	Power-to-X
CAPEX (€ kWh^{-1})	5-100	2-50	600-2500	150-1000	1-10
Roundtrip efficiency (%)	65-85	40-60	85-95	60-85	30-50
LCOES (€ kWh^{-1})	1.4	2.4	-	-	0.5

Table 1: Comparison of CAPEX, roundtrip efficiency and LCOES between storage technologies [29]

The Power-to-Hydrogen (PtH) process involves the use of electricity to convert, by electrolysis, water into hydrogen. One of the advantages of hydrogen is the high gravimetric energy content. Its Lower Heating Value (LHV), which refers to the amount of energy released when a fuel is burned, is the highest compared to the most common fossil fuels, such as gasoline, diesel and methane (CH_4). In addition, H_2 is non-toxic, and its complete combustion produces only H_2O. However, due to its very low density, the volumetric energy density is much lower compared to other fossil fuels, making its storage expensive since bigger volumes are needed (Table 2).

	H_2	Diesel	Gasoline	CH_4
Density (kg m^{-3})	0.089	820	682	0.707
Gravimetric energy density (MJ kg^{-1})	141.9 (HHV) 120 (LHV)	45.4	46.4	56.2 (HHV) 50 (LHV)
Volumetric energy density (MJ L^{-1})	10.1 (HHV) 8.5 (LHV)	34.6	34.2	23.6 (HHV) 20.9 (LHV)

Table 2: Gravimetric and volumetric energy density of common fuels

1.3.2 Hydrogen's limits

Unlike fossil fuels, hydrogen cannot be extracted as an energy-producing resource but must be synthesized. Due to its very low density, hydrogen is rarely available in its molecular state (H_2), and it is almost exclusively found in combination with other chemical elements, such as water (H_2O) and methane (CH_4). To produce hydrogen, therefore, it is necessary to separate it from other elements, and this process consumes energy. Furthermore, additional energy is required to convert hydrogen back into electricity. For these reasons, hydrogen cannot serve as energy source but instead must be used as an energy carrier. Most of the hydrogen is produced via steam methane reforming (SMR), but to play a role in a carbon-neutral energy future, alternative carbon-neutral methods for hydrogen production need to be developed. Different colours are used to describe hydrogen depending on the way it is produced:

- Grey hydrogen → steam methane reforming (SMR)
- Blue hydrogen → steam methane reforming + carbon capture and storage (CCS)

- Green hydrogen → Electrolysis powered by renewable energy
- Black hydrogen → Coal gasification
- Pink hydrogen → Electrolysis powered by nuclear energy

The biggest issues related to hydrogen application are its storage and transport. Hydrogen gas is highly reactive and flammable, so it requires proper controls during production, transport and storage. At the moment there is no adequate infrastructure network able to guarantee its safe distribution. Due to its low density, hydrogen can dissolve quickly into metal at room temperature causing embrittlement in unprotected pipelines. This means that, to transport hydrogen in the existing infrastructure network, significant retrofitting is required. To be efficiently stored and transported, hydrogen needs to be compressed or liquefied. Liquefying hydrogen requires cooling below -253°C, and this process is so energy-intensive that around 44.7% of the initial energy content of the gas phase is lost. [29] Additional energy losses occur due to evaporation, resulting in a storage efficiency of just 21% in seasonal storage applications (182 days). To avoid the high energy of liquefaction, hydrogen can also be stored at pressures ranging between 350 and 700 bar. Storing hydrogen as a compressed gas is relatively efficient (91%), and adequate vessels prevent any leakage, making it suitable also for seasonal applications. However, higher volumes are needed with respect to liquid hydrogen, reducing its applicability. To overcome these problems, other chemicals are to be studied for large-scale efficient and economical H_2 storage and transportation, usually referred as hydrogen carriers.

1.3.3 The role of ammonia

Among different hydrogen carriers, ammonia (NH_3) is a promising candidate because it does not contain carbon, it is not a greenhouse gas and its flammability region in ambient air is very narrow. Furthermore, ammonia contains 17.8% in weight of hydrogen, one of the highest percentages among all hydrogen carriers. Liquefying ammonia requires only cooling below -33°C at atmospheric pressure,

or pressurizing above 7.5 bar at 20°C, with very high efficiency (99%). For this reason, its transport and storage are relatively easy, also considering that existing infrastructures can be exploited. Liquid ammonia has higher energy density compared to liquid hydrogen, meaning that lower volumes are needed to achieve the same energy content (Table 3).

Ammonia also benefits from lower evaporation losses compared to liquid hydrogen, which contributes to a more stable retention of energy content during seasonal storage. Clearly, ammonia offers significant advantages in storage and transportation over liquid hydrogen. However, ammonia storage requires an additional process to extract hydrogen before use, leading to a reduction of the net energy yield for every ton of hydrogen produced. Generally, compression of hydrogen, rather than liquefaction of ammonia and hydrogen, is the more energy efficient method of storing hydrogen. This is mostly due to the evaporation losses that both liquid ammonia and liquid hydrogen face. Anyway, if space and transportation are limiting factors, the use of ammonia is more suitable (Figure 10).

Li-ion battery	Liquid ammonia	Hydrogen at 1 bar, 300 K	Hydrogen at 300 bar, 300 K	Hydrogen at 700 bar, 300 K	Liquefied hydrogen
0.45 MWh m^{-3}	3.58 MWh m^{-3}	0.003 MWh m^{-3}	0.67 MWh m^{-3}	1.34 MWh m^{-3}	2.3 MWh m^{-3}

Table 3: Comparison of energy density of batteries, hydrogen and ammonia [30]

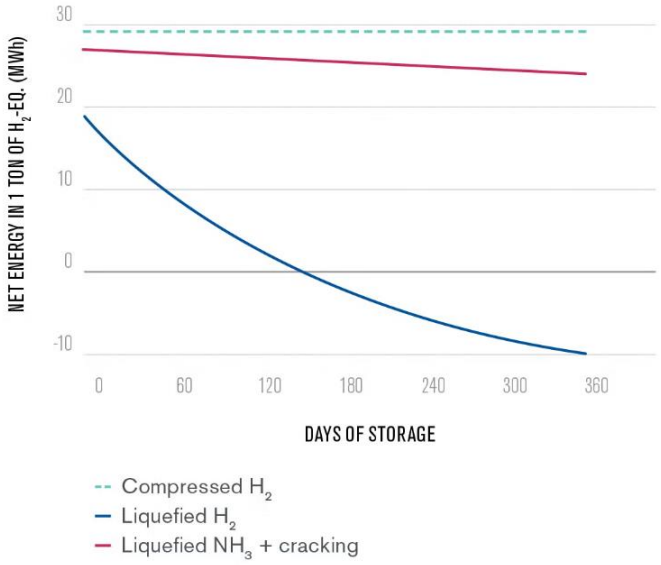

Figure 10: Net remaining energy of hydrogen and ammonia storage over time [30]

Extraction of hydrogen from ammonia can be achieved via ammonia cracking process: [31]

$$2NH_3 \rightarrow N_2 + 3H_2 \qquad \Delta H^0_{298\,K} = 46.22\,\frac{kJ}{mol} \tag{1.11}$$

This process is endothermic and can occur with or without a catalyst. The reaction is favoured at high temperatures and low pressures, so typical temperatures range between 800 °C and 1000 °C. Unlike ammonia synthesis, this technology is not mature. The traditional thermocatalytic ammonia cracking requires high temperatures and noble catalysts. An alternative for ammonia decomposition at lower temperatures consists of amide-imide catalytic systems. Less mature technologies include nonthermal plasma, electrolysis and photocatalysis. After cracking, the gas mixture is passed through a purification system to separate the hydrogen from the nitrogen. Techniques like pressure swing adsorption (PSA) or membrane separation are often used to obtain high-purity hydrogen.

Chapter 2

2. Electrocatalytic reduction of nitrates

2.1 Electrochemical reactors for denitrification

Electrochemical reactors for denitrification are electrolytic cells consisting of at least two electrodes. An electrode is a conductor in contact with electrolytes in aqueous solution. The electrode allows the current circulation through external electrical circuit, and its surface serves to exchange electrons with electroactive species in solution. Electroactive species refer to chemical species that can undergo a redox reaction by direct charge transfer on the electrode's surface. The anode is the electrode where oxidation process takes place, while the cathode is the electrode where reduction takes place. In redox reaction, oxidation and reduction occur simultaneously at the electrode surface. Therefore, a re-oxidation of reduced species could occur at the anode surface. The use of divided cells, such as H-type or flow cells, is considered the most suitable approach because it minimizes the possible re-oxidation at the anode of the reduced species from the cathode. [32]

2.1.1 H-cell vs Flow cell

The H-cell consists of two chambers separated by a porous diaphragm or membrane. The design resembles the shape of the letter "H" when viewed from above (Figure 11). The electrolyte is typically static in each chamber, meaning that the solution does not flow through the system. H-cells are suited for controlled experiments where the focus is on the reaction kinetics in a static environment, but they are limited to processes that do not require continuous flow or replenishment of reagents. On the other hand, a flow cell has a more dynamic design. A flow cell is designed so that the liquid electrolyte can be continuously flowed through the beam path. Flow cell electrolysers are essential tools for the scale-up of

electrocatalytic processes. They offer more control over reagent delivery, improving the mass transport and thus generating current densities significantly higher. [33] However, flow cells have a more complex design than H-cells and typically require pumps, making them more prone to issues like clogging and leakage. In summary, H-cells are suited for more controlled, static experiments, while flow cells are suited for dynamic, continuous processes.

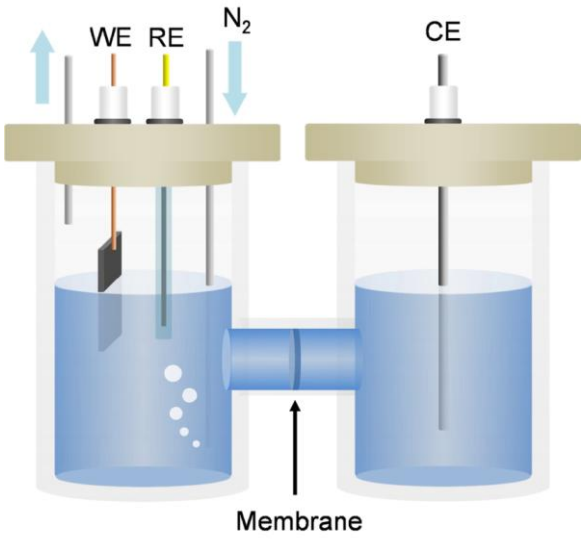

Figure 11: Schematic illustration of H-cell [34]

2.1.2 Ion exchange membrane

In divided electrolytic cells, the anode and the cathode are physically separated in two chambers. The two chambers are typically separated by an ion exchange membrane, which allows the selective passage of certain ions while blocking others. There are two main types of ion exchange membranes: Cation Exchange Membranes (CEMs), which allow the movement of cations and block anions, and Anion Exchange Membranes (AEMs), which allow the movement of anions and

block cations. In the case of denitrification, CEMs are used to separate the anode and cathode compartments. These membranes allow the transport of protons (H^+) and block anions like nitrate (NO_3^-) and nitrite (NO_2^-). Nafion membranes are the most used for this application. Nafion is a sulphonated tetrafluorethylene polymer that consists of a hydrophobic fluorocarbon backbone ($-CF_2-CF_2-$) and hydrophilic sulphonate groups (SO_3^-) that are attached to this backbone (Figure 12). Divided electrolytic cells with Nafion membranes show high nitrate reduction efficiency, with removal rates increasing proportionally to current density, preventing the re-oxidation of nitrite produced during the reduction process. [35] However, recent research has highlighted potential drawbacks of Nafion membranes, including ammonium ion absorption and release, which can affect ammonia production measurements. To solve these problems, alternative separators like Zirfon and Celgard have been proposed, showing less interaction with ammonia. ([36], [37])

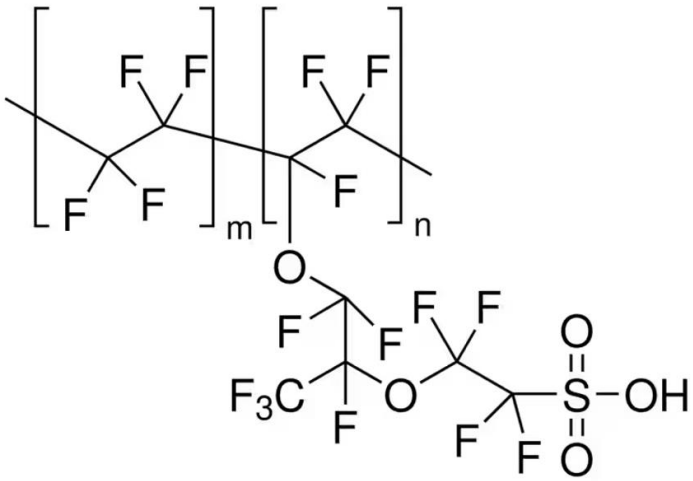

Figure 12: Chemical structure of Nafion membrane [38]

2.1.3 Electrolyte

The electrolyte serves as the medium through which ions move, enabling the electrochemical reactions at the anode and cathode to proceed efficiently. The

choice of the electrolyte depends on several factors, including the type of denitrification process (e.g. nitrate reduction to nitrogen gas, nitrite, or ammonia), the electrode material, and the operating conditions of the electrochemical cell. The electrolyte must have adequate ionic conductivity to allow the efficient ions flow between the cathode and the anode. Nitrate salts are commonly used because they provide a good balance of conductivity and nitrate concentration. Aqueous electrolytes are water-based solutions containing dissolved nitrate ions, usually in form of salts like sodium nitrate ($NaNO_3$) or potassium nitrate (KNO_3). These salts provide a source of nitrate for reduction at the cathode. In some denitrification systems, acidic electrolytes (e.g. H_2SO_4, HCl) are used. These acids provide a source of protons, which are required for the reduction of nitrate at the cathode. Acidic conditions favour the nitrate reduction reaction to nitrogen gas and reduce the chance of nitrate reduction to ammonia. Alkaline electrolytes (e.g. NaOH, KOH) can also be used, especially in cases where the reduction of nitrate to ammonia is targeted. In fact, alkaline conditions favour the nitrate reduction reaction to ammonia rather than nitrogen gas, as ammonia is more stable in a basic environment.

2.1.4 Electrodes

In electrochemical denitrification, electrodes play a central role in facilitating the reduction of nitrate at the cathode, and oxidation at the anode. To control the electrode potential, a three-electrode system is required: a working electrode, a counter electrode and a reference electrode. The working electrode is the cathode where the reduction occurs. An ideal cathode should have high catalytic activity for nitrate reduction, good electrical conductivity to facilitate electron transfer, chemical stability to resist degradation and corrosion over time, and the ability to support efficient gas evolution. Carbon-based materials, such as Graphite, are widely used because of their low costs and good electrical conductivity. An interesting carbon-based material is the carbon paper; this material has high surface area, which enhance the efficiency of the denitrification process by increasing the

contact area for electrochemical reactions. [39] Copper electrodes can also be used for nitrate reduction and are relatively cost-effective, especially when modified with catalysts that promote selective nitrate reduction to nitrogen gas, such as Palladium. [40] Together with the working electrode, the counter electrode completes the electrical circuit. In the case of denitrification process, the counter electrode is the anode. An ideal anode should have stability in oxidative conditions, high electrical conductivity and good electrocatalytic activity for oxygen evolution. Platinum is commonly used as an anode in electrochemical cells due to its high stability and efficiency for oxygen evolution reactions. However, like platinum cathodes, platinum anodes are expensive and not suited for large-scale applications. Titanium coated with iridium oxide (IrO_2) and lead dioxide (PbO_2) are often used due to their high stability and good catalytic properties. Also carbon-based materials, such as graphite, are used because of their low cost and good electrical conductivity; however, graphite anodes may suffer from oxidative degradation, thus limiting their applicability.

The reference electrode is used as a reference point against which the potential of the working electrode can be measured. It has a well-defined and stable equilibrium potential. Several types of reference electrodes can be employed in electrochemical denitrification setups, each with specific advantages based on the experimental conditions. The Saturated Calomel Electrode (SCE) consists of mercury and mercury chloride in a saturated potassium chloride solution. It is stable and provides a reference potential of 0.241 V*vs*SHE. [41] The main disadvantage is that it requires the handling of toxic mercury and may not be suitable for certain environments where mercury contamination is a concern. The Ag/AgCl is another commonly used reference electrode. It consists of silver (Ag) coated with silver chloride (AgCl) immersed in a potassium chloride (KCl) solution (Figure 13).

It is easier to handle, cheaper and more environmentally friendly than SCE, but is less stable under certain conditions, especially when the chloride concentration is low.

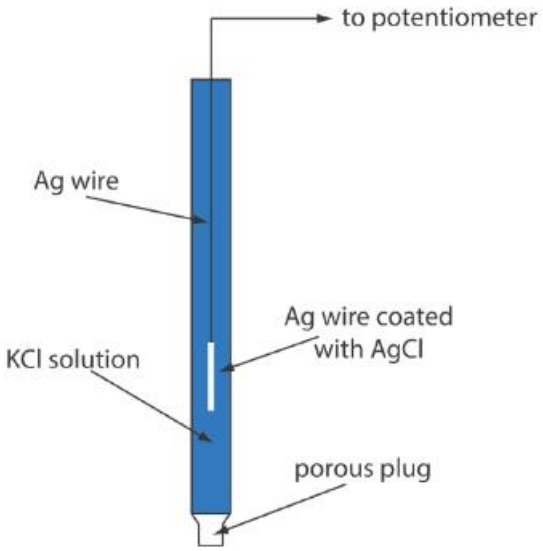

Figure 13: Schematic diagram of Ag/AgCl electrode [41]

2.1.5 Catalysts

The catalyst plays a crucial role in facilitating the reduction of nitrate to nitrogen gas or ammonia. It helps accelerate the electrochemical reactions at the electrodes, promoting the transfer of electrons and improving the efficiency of nitrate removal. A wide range of materials as catalysts have been used in electrochemical denitrification. Platinum is a widely used catalyst because of its excellent conductivity and high resistance to corrosion. However, platinum is expensive, and researchers often try to find alternative materials or platinum-based alloys for cost reduction while maintaining efficiency. Transition metals like Palladium (Pd), copper (Cu), and iron (Fe) are commonly used due to their strong catalytic activity. For example, Pd-based catalysts are highly effective in breaking the N-O bond, while Cu is known for its ability to promote the reduction of nitrite to nitrogen. Bimetallic catalysts, such as Pd-Cu and Pt-Sn, have gained significant attention because of their synergistic effects, where one metal enhances nitrate adsorption and the other facilitates electron transfer. Carbon-based materials, including carbon

nanotubes (CNTs), graphene, and activated carbon, are often used as catalyst supports due to their high surface area, excellent electrical conductivity and chemical stability. These materials can be further functionalized or doped with metals to enhance their catalytic properties. For instance, nitrogen-doped graphene has shown improved performance in electrochemical denitrification due to its ability to facilitate electron transfer and provide active sites for nitrate adsorption.

2.2 Reaction mechanisms

The mechanisms for electrochemical conversion of nitrate to nitrogen gas involve different reactions, products and intermediates.

The Frost-Ebsworth diagram illustrates the relative stability of different oxidation states of a nitrogen species (Figure 14). The diagram shows on its X-axis the oxidation state of the species in question, and on its Y-axis the ratio between the Gibbs free energy of the half-reduction reaction of the species (ΔG°) and the faraday constant (F). The slope of the line between any two points of the diagram gives the standard reduction potential E° for the corresponding half-reaction. From the diagram it is observed that N_2 and NH_3/NH_4^+ are the thermodynamically most stable forms of nitrogen under standard conditions. However, different factors can modify the final products of electrochemical reduction and the pathway of the reactions. The overall reaction mechanisms of the electrochemical reduction of nitrates can be divided into different mechanisms (Figure 15).

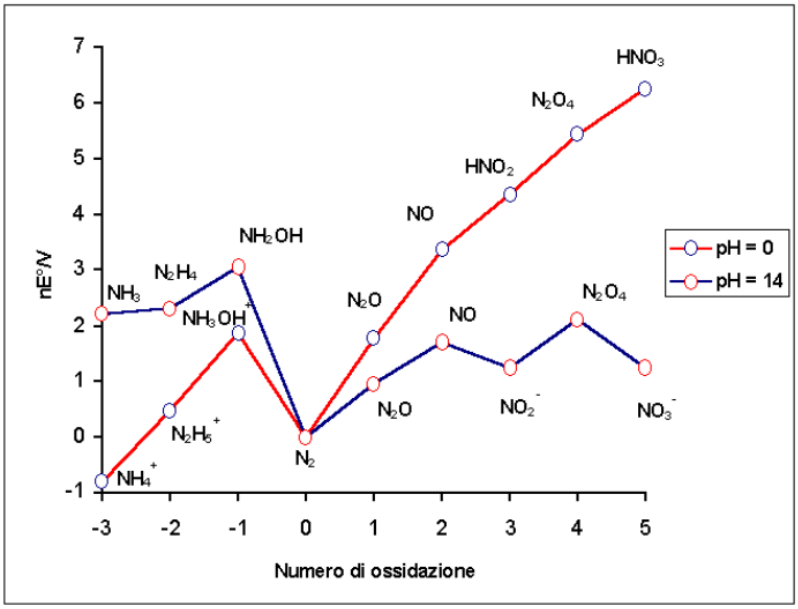

Figure 14: Frost-Ebsworth diagram for nitrogen at different pH levels [42]

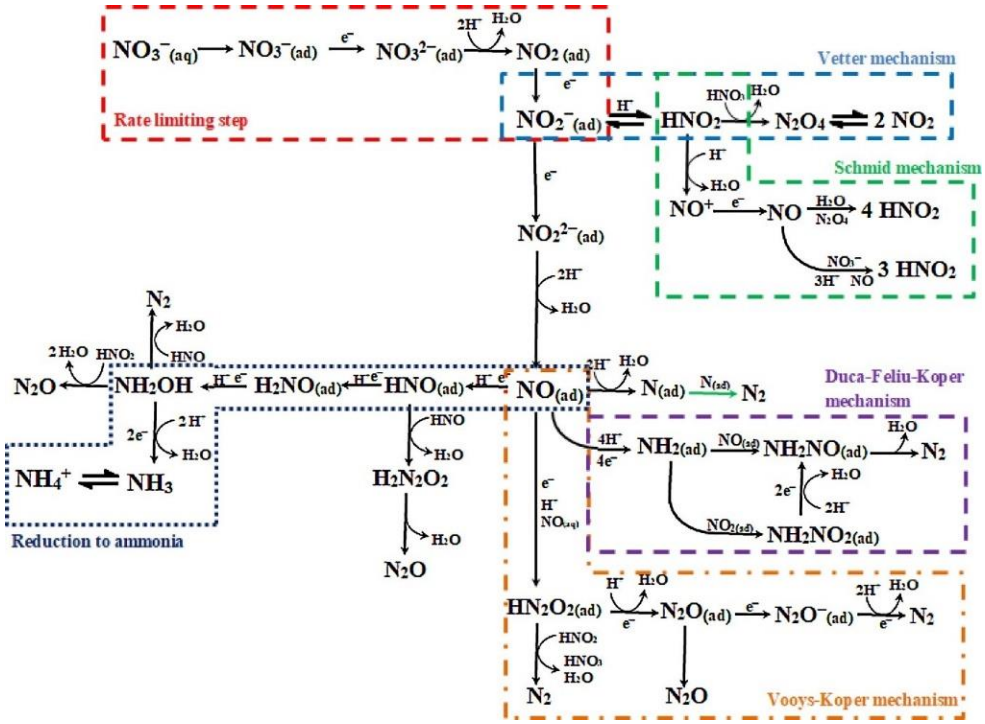

Figure 15: mechanisms of electrochemical reduction of nitrates [32]

The electrochemical production of NH_3 from NO_3^- follows an eight-electron transfer process, with oxidation states ranging from +5 in NO_3^- to -3 in NH_3. The reduction of nitrate (NO_3^-) into nitrite (NO_2^-) is the rate-limiting step. It requires an initial adsorption step onto the cathode surface, and co-adsorbing ions from solution inhibit the overall reduction. [43] Thus, mass transfer of nitrate from bulk to the electrode surface limits nitrate adsorption, surface-bound nitrate concentrations and consequently overall electrochemical nitrate reduction rate. Electrochemical nitrate reduction is a mass transfer limited process, and consequently the nitrate concentration is relevant because it defines the diffusion rate from the solution towards the cathode surface according to Fick's law:

$$J = -D\frac{dC}{dx} \tag{2.1}$$

Where J is the diffusion rate, expressed in mol m^{-2} s^{-1}, and is the amount of substance that diffuses through a unit area per unit of time; D is the diffusion coefficient, expressed in m^2 s^{-1}, and $\frac{dC}{dx}$ is the concentration gradient, expressed in mol m^{-3} m^{-1}. The higher the nitrate concentration, the higher will be the diffusion rate.

The electrochemical reduction of adsorbed nitrate to nitrite involves a three-step electrochemical-chemical-electrochemical (ECE) mechanism. In ECE mechanisms, the first electron transfer mechanism is firstly followed by a chemical reaction that produces reducible species and lastly by a second electron transfer reaction. The first step is the reduction of the adsorbed NO_3^- into a nitrate di-anion radical (NO_3^{2-}), followed by a chemical reaction that leads to the formation of nitrogen dioxide radical ($NO_2\cdot$), and finally another reduction into NO_2^-.

$$NO_{3\,(ad)}^{-} + e^{-} \rightarrow NO_{3\,(ad)}^{2-} \tag{2.2}$$

$$NO_{3\,(ad)}^{2-} + H_2O \rightarrow NO_2\,\cdot_{(ad)} + 2OH^- \quad (2.3)$$

$$NO_2\,\cdot_{(ad)} + e^- \rightarrow NO_{2\,(ad)}^- + H_2O \quad (2.4)$$

The nitrate electroreduction is divided into two parts: the indirect autocatalytic reduction pathway and the direct electrocatalytic reduction pathway (Figure 16). The indirect autocatalytic reduction is considered an indirect reduction mechanism because the nitrate is not the electroactive species, although the overall reaction reduces nitrate to nitrous acid. The direct electrocatalytic reduction includes two pathways: the adsorbed-hydrogen-mediated pathway and the electron-mediated pathway.

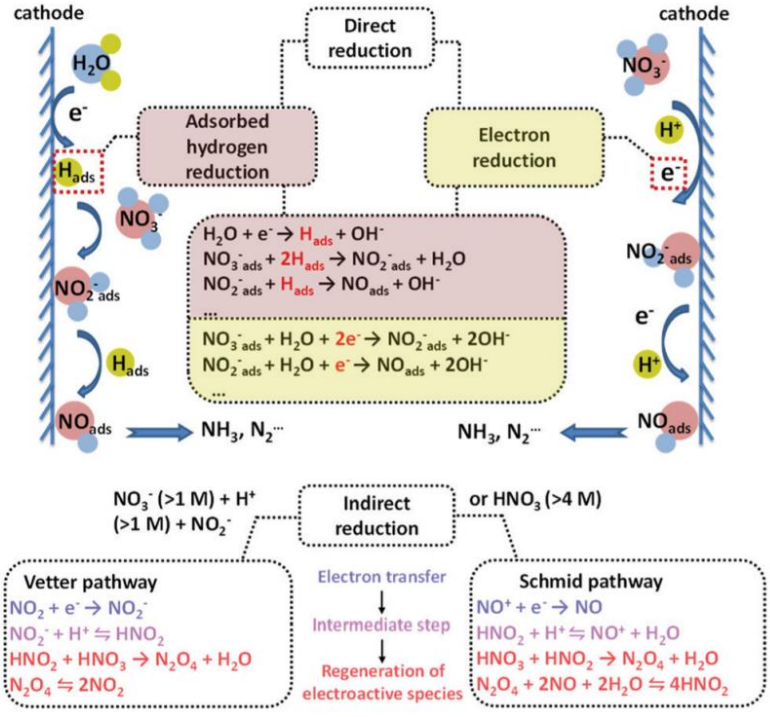

Figure 16: The different pathways of nitrate electroreduction [44]

2.2.1 Indirect autocatalytic reduction pathway

Under highly acidic conditions and high reactant concentrations (1.0–4.0 M NO_3^-), the adsorbed nitrite ion is protonated into nitrous acid (HNO_2), inducing two autocatalytic mechanisms: Vetter mechanism and Schmid mechanism. This mechanism is important because it can accelerate the nitrate reduction rates and increase faradaic efficiencies. [32]

The Vetter mechanism involves NO_2· as the electroactive species in the autocatalytic cycle. The nitrite anion protonates to nitrous acid following an acid base-equilibration under highly acidic conditions. The nitrous acid reacts with nitric acid (HNO_3), resulting in H_2O and dinitrogen tetraoxide (N_2O_4) that is quickly reduced, releasing two electroactive NO_2· species. In brief, each NO_2· species entering the autocatalytic cycle generates two NO_2·.

$$NO_2^- + H^+ \leftrightarrow HNO_2 \tag{2.5}$$

$$HNO_2 + HNO_3 \rightarrow N_2O_4 + H_2O \tag{2.6}$$

$$N_2O_4 \leftrightarrow 2NO_2 \cdot \tag{2.7}$$

In contrast, the Schmid mechanism involves nitrosonium cation (NO^+) as the electroactive species in the autocatalytic cycle. The NO^+ originates from the protonation of nitrous acid in highly acidic environment. NO^+ is electrochemically reduced to NO and further converted to HNO_2. Here, two options are possible: two NO species react with N_2O_4 in aqueous media leading to formation of 4 mol of HNO_2, or nitric acid directly reacts with two NO species to yield 3 mol of HNO_2 (Abel pathway).

$$HNO_2 + H^+ \leftrightarrow NO^+ + H_2O \quad (2.8)$$

$$NO^+ + e^- \leftrightarrow NO \quad (2.9)$$

$$N_2O_4 + 2NO + 2H_2O \leftrightarrow 4HNO_2 \quad (2.10)$$

$$HNO_3 + 2NO + H_2O \leftrightarrow 3HNO_2 \quad (2.11)$$

2.2.2 Direct electron-mediated pathway

The previous pathways are preferred when NO_2^- is unstable. However, if the adsorbed NO_2^- is stable, the preferred pathway is different. The adsorbed nitrite anion is reduced by direct charge transfer reaction, leading to the formation of the dianion radical NO_2^{2-}, which quickly hydrolyzes and produces adsorbed NO.

$$NO_{2\,(ad)}^- + e^- \rightarrow NO_{2\,(ad)}^{2-} \quad (2.12)$$

$$NO_{2\,(ad)}^{2-} + H_2O \rightarrow NO_{(ad)} + 2OH^- \quad (2.13)$$

These steps are influenced by the adsorption energy of $NO_{(ad)}$ on the catalyst. If the adsorption energy is high the catalyst is poisoned, while if it is low that can lead to the desorption of $NO_{(ad)}$ [45]. One possible pathway is the reduction of the adsorbed NO into adsorbed atomic nitrogen ($N_{(ad)}$), which then reacts with a second nitrogen atom to form the triple bond of nitrogen.

$$NO_{(ad)} + 2H^+ + 2e^- \rightarrow N_{(ad)} + H_2O \quad (2.14)$$

$$N_{(ad)} + N_{(ad)} \rightarrow N_2 \quad (2.15)$$

The Vooys-Koper mechanism considers an initial elementary electrochemical reaction involving adsorbed and dissolved NO that forms diazeniumdiolate (HN_2O_2). HN_2O_2 is then easily reduced by a second charge transfer to yield N_2O. The formed N_2O can be further reduced to N_2O^-, that can be finally reduced to N_2.

$$NO_{(ad)} + NO_{(aq)} + H^+ + e^- \rightarrow HN_2O_2 \quad (2.16)$$

$$HN_2O_{2(ad)} + H^+ + e^- \rightarrow N_2O_{(ad)} + H_2O \quad (2.17)$$

$$N_2O + e^- \rightarrow N_2O^- \quad (2.18)$$

$$N_2O^- + 2H^+ + e^- \rightarrow N_2 + H_2O \quad (2.19)$$

Another possible pathway is the Duca-Feliu-Koper mechanism. This pathway involves the hydrogenation of $NO_{(ad)}$ in a basic solution to $NH_{2\,(ad)}$, followed by the reaction between adsorbed NO and $NH_{2\,(ad)}$ to form N-nitrosamide ($NONH_2$), which then decomposes to generate N_2.

$$NO_{(ad)} + NH_{2\,(ad)} \rightarrow NONH_{2\,(ad)} \quad (2.20)$$

$$NONH_{2\,(ad)} \rightarrow N_2 + H_2O \quad (2.21)$$

The last major product yielded during the electrochemical nitrite reduction is ammonia (NH_3/NH_4^+). The reduction of NO leads to the formation of azanone (HNO). Then HNO is reduced to H_2NO, quickly followed by an additional charge transfer releasing hydroxylamine (H_2NOH). Finally, ammonia is produced from the fast electrochemical reduction of hydroxylamine. Ammonia is in equilibrium with ammonium ion; this means that they are interconverting back and forth in a reversible chemical reaction, and the concentration of both remain constant over time.

$$NO_{(ad)} + H^+ + e^- \leftrightarrow HNO_{(ad)} \quad (2.22)$$

$$HNO_{(ad)} + H^+ + e^- \rightarrow H_2NO_{(ad)} \quad (2.23)$$

$$H_2NO_{(ad)} + H^+ + e^- \rightarrow H_2NOH_{(ad)} \quad (2.24)$$

$$H_2NOH + 2H^+ + 2e^- \rightarrow NH_3 + H_2O \quad (2.25)$$

$$NH_3 + H^+ \leftrightarrow NH_4^+ \quad (2.26)$$

2.2.3 Direct adsorbed-hydrogen-mediated pathway

The adsorption of molecular hydrogen (H_2) can inhibit the electrocatalytic reduction of nitrate [46], but the ammonia production can be enhanced because hydrogen promotes N-H bond formation instead of N-N triple bond. During this pathway, water is reduced to stable adsorbed hydrogen ($H_{(ad)}$) on the cathode surface, that recombines into molecular hydrogen.

$$H_2O + e^- \rightarrow H_{(ad)} + OH^- \quad (2.27)$$

$$H_{(ad)} + H_{(ad)} \rightarrow H_2 \quad (2.28)$$

Then, $H_{(ad)}$ directly reduces nitrate to NH_4^+ via intermediates such as $NO_2^-{}_{(ad)}$, $NO_{(ad)}$ and $N_{(ad)}$. The reactions are the following:

$$NO_{3\,(ad)}^- + 2H_{(ad)} \rightarrow NO_{2\,(ad)}^- + H_2O \quad (2.29)$$

$$NO_{2\,(ad)}^- + H_{(ad)} \rightarrow NO_{(ad)} + OH^- \quad (2.30)$$

$$NO_{(ad)} + 2H_{(ad)} \rightarrow N_{(ad)} + H_2O \quad (2.31)$$

$$N_{(ad)} + H_{(ad)} \rightarrow NH_{(ad)} \quad (2.32)$$

$$NH_{(ad)} + H_{(ad)} \rightarrow NH_{2\,(ad)} \quad (2.33)$$

$$NH_{2\,(ad)} + H_{(ad)} \rightarrow NH_{3\,(ad)} \quad (2.34)$$

Strong competition from HER presents a significant challenge in aqueous systems. At pH = 0, the formation of H_2 requires only 0.25 eV, lower than the 0.37 eV needed for nitrate reduction, making the NO_3RR less favourable in acidic conditions. However, in neutral conditions (pH = 7), NO_3RR is more favourable than HER. [47] This indicates that pH significantly influences the competition between HER and NO_3RR.

2.3 Reaction parameters

2.3.1 pH

The pH of the electrolyte solution plays a critical role in the electrocatalytic reduction of nitrates, as it influences reaction mechanisms, selectivity, efficiency, and by-product formation. In acidic conditions (pH<7), protons are abundant, and the high proton availability accelerates the reduction process. An electrolyte with low pH facilitates the formation of ions which can reduce nitrates and nitrites. [48] On the other hand, the Pourbaix diagram shows that the HER cannot be ignored as it competes with the electrochemical nitrate reduction. The Pourbaix diagram illustrates the stability regions of different phases of a chemical species as a function of both electrode potential and pH (Figure 17). The diagram shows on its X-axis the pH of the solution, ranging from acidic on the left to basic on the right, and on its Y-axis the standard reduction potential.

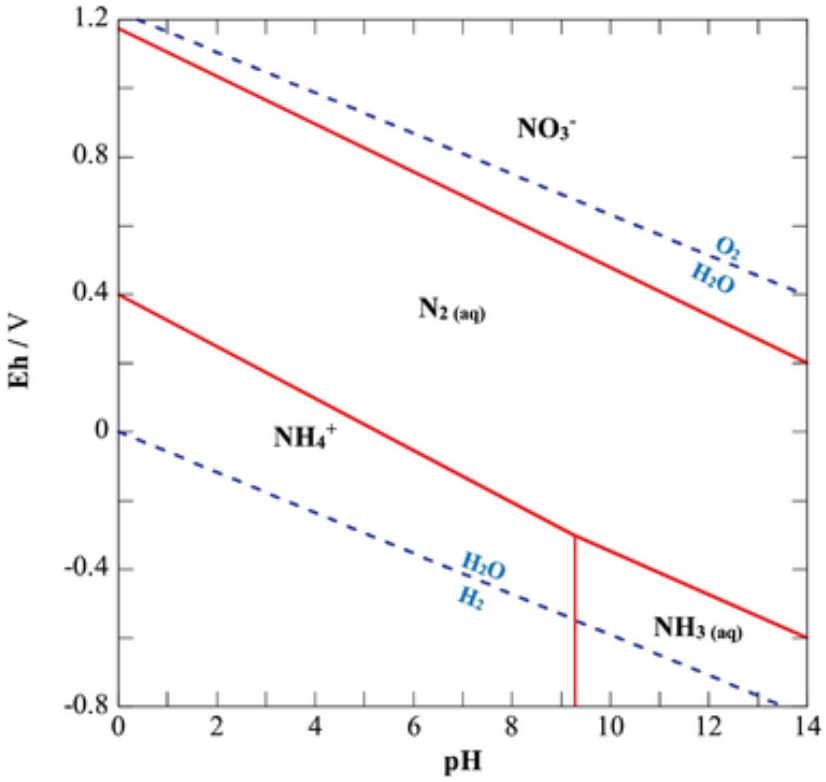

Figure 17: Pourbaix diagram of nitrogen species [49]

From the diagram it is observed that HER is increased at low pH, resulting in hydrogen bubbles formation that prevents the contact between the active site and the electrolyte and thus a reduction of the faradaic efficiency (FE) of nitrate reduction. During the reduction process, protons are consumed and so the pH of the solution increases. In alkaline conditions (pH>7), the lack of protons can limit the reduction of nitrate and nitrite, favouring the formation of ammonia. In an electrolyte with high pH the HER is less competitive, but adsorbed hydroxide ions may occupy active sites on the electrode, reducing its effectiveness. For these reasons, an electrolyte with neutral pH (≈7) is the most favourable for electrocatalytic nitrate reduction. [50] Therefore, the optimal pH must be carefully selected based on the specific requirements of the process.

pH condition	Nitrate reduction efficiency	HER competition	By-product formation	Remarks
Acidic (pH < 7)	High (due to proton availability)	High	N_2, N_2O favoured; NH_3 minimized	Best for nitrate removal but suffers from HER
Neutral (pH = 7)	Moderate to high	Moderate	N_2, N_2O favoured; NH_3 minimized	Balanced conditions for efficiency and selectivity
Alkaline (pH > 7)	Low (due to proton limitation)	Low	N_2, N_2O minimized; NH_3 favoured	Less competitive HER but favours ammonia formation

Table 4: Summary of pH effects on electrocatalytic reduction of nitrates

2.3.2 Nitrate concentration

The concentration of nitrate in the solution can affect the efficiency, selectivity, and reaction mechanisms of the process. The variation in nitrate concentration causes changes in the kinetic order of the electrode during the reduction. Generally, increasing the initial nitrate concentration can enhance the reaction due to a higher availability of nitrate ions at the electrode surface, leading to higher kinetics and higher current density. At low concentration, the reaction may be limited by mass

transport of nitrate ions to the electrode surface, resulting in lower kinetics and lower efficiency.

2.3.3 Applied voltage and current density

The applied voltage or potential has a relatively strong effect on nitrate reduction. A minimum voltage is required to initiate the reaction. This depends on the electrode material and electrolyte composition. Increasing the applied voltage generally accelerates the reaction rate by providing more energy to overcome activation barriers. However, excessively high voltages can lead to side reactions, such as HER, reducing the faradaic efficiency for nitrate reduction. Also, the selectivity of nitrate reduction in products is strongly dependent on the potential applied. [51] Higher voltage means also higher energy consumption; therefore, this aspect must be taken into account when considering the benefits of the overall process. In addition to the applied potential, the current density also plays a significant role in the performance of nitrate removal. Higher current densities generally increase the rate of nitrate reduction by providing more electrons for the reaction. The nitrate removal efficiency increases progressively with increasing current density. [48] However, mass transport limitations can become significant at very high current densities. Furthermore, very high densities can cause electrode degradation, reducing the long-term performance of the system.

2.3.4 Coexisting ions

In the context of electrochemical processes, coexisting ions refers to other ions present in the electrolyte alongside the target species (e.g. nitrate). These ions can originate from the electrolyte itself, the water source, or added chemicals. Coexisting ions can significantly influence the efficiency, selectivity, and overall performance of the electrochemical process.

Coexisting ions can be categorized based on their charge and chemical nature:

- Cations (e.g. Na^+, K^+, Ca^{2+}, Mg^+)
- Anions (e.g. Cl^-, SO_4^{2-}, HCO_3^-, PO_4^{3-})
- Organic ions (e.g. acetate, formate, or humic acids)

Coexisting ions like Na^+ and K^+ can increase the ionic strength and conductivity of the electrolyte, improving charge transfer and reducing energy consumption. The cation of the supporting electrolyte acts as a centre for the reduced anion by forming an instantly neutral ion pair. The latter is not repelled by the negatively charged electrode, increasing the rate of nitrate reduction. [43] Ions like HCO_3^- and CO_3^{2-} can act as pH buffers, stabilizing the electrolyte pH and preventing extreme acidic or alkaline conditions that could alter the reaction pathways. Certain ions like Fe^{2+} and Cu^{2+} can act as catalysts or co-catalysts, enhancing the rate of nitrate reduction or improving selectivity toward desired products. However, other ions can have negative effects on the performance of the process. For example, chloride ions, which are the primary ions present in brackish groundwater, can limit the reaction. This is due to the fact that chlorine ion oxidations reactions (CIOR) have higher potential with respect to oxygen evolution reactions (OER) at the anode. In acidic conditions, ClOR manifests as a chlorine evolution reaction (ClER), while in alkaline conditions, it forms hypochlorite, both of which are corrosive and detrimental to catalyst longevity. [52] In high pH environments, divalent cations like Ca^{2+} and Mg^{2+} can form insoluble precipitates on the electrode surface, leading to scaling and fouling.

Chapter 3

3. Materials and methods

3.1 Materials

The following materials were purchased from Quintech:

- Nafion membranes (Nafion 117, N-117) with a nominal thickness of 183 μm
- Carbon paper (Toray paper 060, N1S1007, AvCarb MGL 190), used as electrode support

The following materials were purchased from Sigma-Aldrich:

- Sodium and potassium sulphates (Na_2SO_4 and K_2SO_4, ≥99.0%), used to prepare electrolytes
- Sulfuric acid (H_2SO_4, 95.0% - 98.0%), used as trap for NH_3
- Potassium hydroxide (KOH, ≥85.0%), used to modify the pH of the solutions
- Sodium citrate dihydrate (HOC(COONa) $(CH_2COONa)_2 \cdot 2H_2O$, ≥99.0%), sodium salicylate ($C_7H_5NaO_3$, 99.5%), sodium nitroferricyanide (III) dihydrate ($Na_2[Fe(CN)_5NO] \cdot 2H_2O$, 99.0%), sodium hypochlorite (NaClO, 5% active chlorine), and sodium hydroxide (NaOH, ≥97.0%), used to measure the NH4 + concentration in the electrolyte via the salicylate method
- Sodium and potassium nitrates (KNO_3 and $NaNO_3$, ≥99.0%), used as nitrate source
- Commercial molybdenum disulfide powder (MoS_2, <2μm, 99.0%), used as catalyst
- Nafion perfluorinated resin solution

All the solutions were prepared with ultrapure water (Milli-Q) produced by a Rephile Genie U Ultrapure & RO lab water system.
The micro-flow-cell was purchased from ElectroCell.

3.2 Experimental setup

A commercial micro-flow-cell reactor was used for the tests. The flow cell components are shown in Figure 18: the cathode and the reference electrode are on the same side of the cell and the catholyte passes through their channels; the anode is on the other side of the cell and the anolyte passes through its channels; the two sections are separated with a Nafion 117 membrane; each component of the cell is separated using a gasket, which prevent the leakage while under compression; the cell is closed between two Teflon guides that allow an easier assembly of the components, and between two stainless steel support.

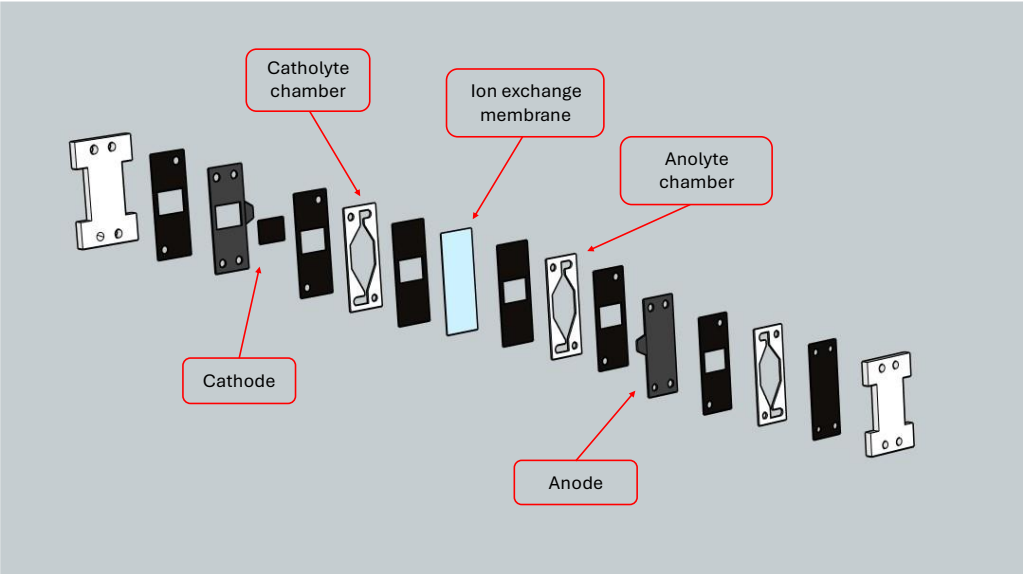

Figure 18: Flow cell exploded scheme

The respective electrolytes (anolyte and catholyte) were continuously recirculated from reservoir bottles through a peristaltic pump (Ismatec™ Reglo ICC) at a flow rate of 20 mL min^{-1}. The catholyte and anolyte total volume was 50 mL and reservoir bottles were sealed to avoid possible NH_3 losses. Electrolytes were purged with inert gas (Argon) before circulating in the cell to pull out undesired and reactive gases such as oxygen and carbon dioxide. The electrodes were all connected to a VSP-300 potentiostat (Biologic VSP-300) to perform the electrochemical tests. The potentiostat was used to control the applied potential of the working electrode as a function of the reference electrode potential. An acid trap consisting of 25 mL of H_2SO_4 0.02 M was connected to the catholyte reservoir bottle to recover the possible volatilized NH_3 (Figure 19).

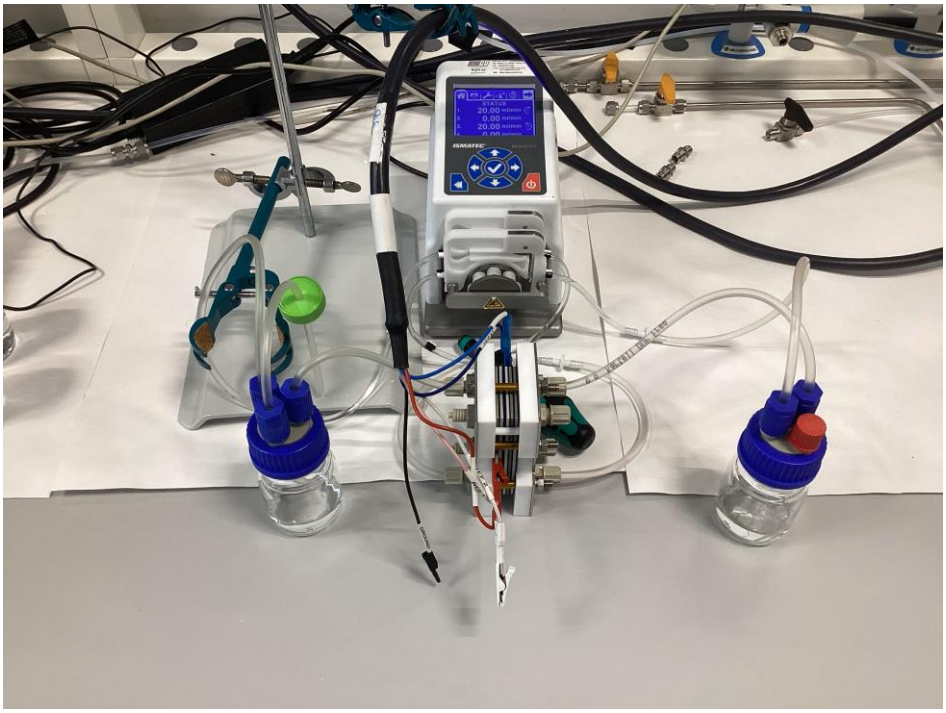

Figure 19: flow cell configuration

3.3 Procedure

First, the ideal cathode support to be used in the experiment was selected. Different types of carbon paper as support for the cathode were tested:

- Toray Paper 060 (0.19 mm thickness – 20%wt PTFE treated) (Figure 20)
- N1S1007 (0.21 mm thickness – with microporous layer and PTFE treated)
- AvCarb MGL 190 (0.19 mm thickness – hydrophilic and no PTFE treated)

The cathode active area was 10.2 cm^2 (different to the actual electrode area which was 10.5 cm^2). A mixed metal oxide electrode with iridium was used as counter electrode, while a leak-free Ag/AgCl electrode, place close to the cathode, was used as reference electrode. The catalyst used was commercial MoS_2. Based on previous experiments, the best performance is achieved when the catalyst loading is 1 mg/cm^2. Therefore, to get such catalyst loading, an ink was prepared and sprayed all over the carbon paper using a compressed air gun. The ink consisted of carbon black, MoS_2, Nafion solution and ethanol. The proportion between the components of the ink is listed in Table 5. The carbon black has the function of increasing conductivity. The Nafion perfluorinated resin solution acts as a binder, while the ethanol is the solvent. The ink was mixed up using an Ultrasonic processor (SONICS, VCX130PB) for 15 minutes. The catalyst loading was calculated as follows:

$$m_{solids} = m_{catalyst} + m_{carbon\_black} + 0.05 \cdot m_{nafion\_solution} \quad (3.1)$$

$$\%_{catalyst} = \frac{m_{catalyst}}{m_{solids}} \quad (3.2)$$

$$m_{catalyst\_deposited} = \%_{catalyst} \cdot m_{deposited} \quad (3.3)$$

$$catalyst\ loading = \frac{m_{catalyst\_deposited}}{A_{electrode}} \quad (3.4)$$

All the masses were measured using a precision balance with an error of ±0.00001 g. The deposited mass was calculated with the formula:

$$m_{deposited} = m_{electrode_{final}} - m_{electrode\_initial} \quad (3.5)$$

Figure 20: an example of carbon paper (Toray Paper 060) [53]

Ratio Solid (catalyst + CB): Binder (nafion)	
Solids	70%
Nafion	30%
Ratio solvent: solids (catalyst + CB + nafion)	wt%
Ethanol	97%
Naf+cat	3.00%

Table 5: ink components proportion

After the cathode support was selected, different electrolytes were tested:

- K_2SO_4 0.3 M + NO_3^- 8 mM → optimum obtained in a previous work of the group for the same catalyst and cell architecture
- Na_2SO_4 0.3 M + NO_3^- 8 mM → to evaluate the effect of the cation in the supporting salt
- Na_2SO_4 12.5 mM + NO_3^- 2 mM → values similar to those found in brackish groundwaters
- Na_2SO_4 0.1 M + NO_3^- 6 mM → values similar to those measured for brackish groundwater RO brine
- Na_2SO_4 0.3 M + NO_3^- 6 mM → to evaluate the effect of Na_2SO_4 concentration

Then, the analysis of a simulated brackish groundwater RO brine was performed, considering the single effect of different elements present in the water. The elements are listed in the Table 6. In the end, to simulate real conditions of real water, the analysis of the combined effects of these elements was performed.

Element	**Concentration (mg L^{-1})**
K^+	74
Mg^{2+}	157
Ca^{2+}	567
HCO_3^-	417
Cl^-	5522
F^-	4
PO_4^{3-}	0.4
SiO_2	50
Humic Acids	4

Table 6: list of brackish groundwater RO brine components [54]

3.3 Electrochemical protocol

The experiment was performed according to an electrochemical protocol which consists of:

- Open circuit voltammetry (OCV)
- Cyclic voltammetry (CV)
- Linear sweep voltammetry (LSV)
- Chronoamperometry (CA) or Chronopotentiometry (CP)

The electrolytes were substituted by "fresh" electrolytes after the LSV, to avoid the presence of NH_4^+ before starting the CA or CP, and to start the test always at the same NO_3^- concentration. Samples were taken before and after the CA or CP from both cathodic and anodic sides.

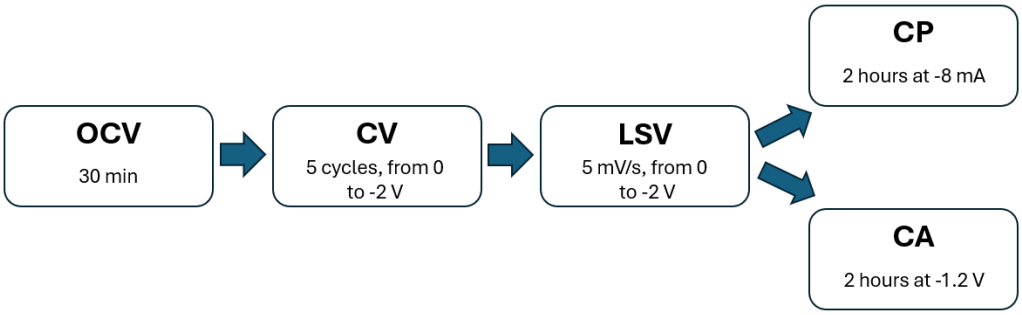

Figure 21: test protocol

3.3.1 Open circuit voltammetry (OCV)

Open circuit voltammetry is a method in which the potential established between the working electrode (cathode) and the environment, with respect to the reference electrode, is measured. This measurement consists in the registration of the evolution of the rest potential, when no current flow through the cell and any potential is applied to the electrode against a reference electrode. The OCV is used

to allow the system stabilizing for a short period before applying another electrochemical technique. [55] For this experiment, an OCV lasting 30 minutes was performed prior to any other techniques. The following figure shows an example of the output of the OCV, with the time on the X-axis and the working electrode potential on the Y-axis (Figure 22).

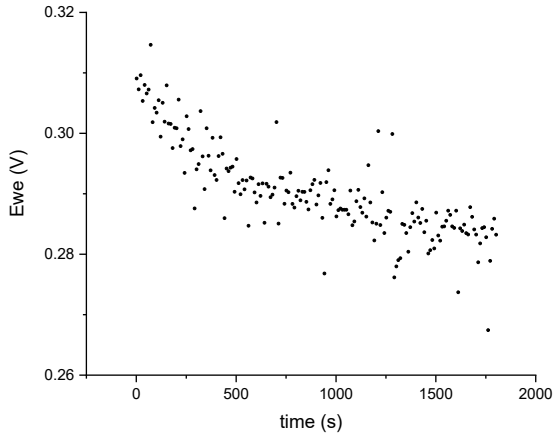

Figure 22: example of an Open Circuit Voltammetry (OCV)

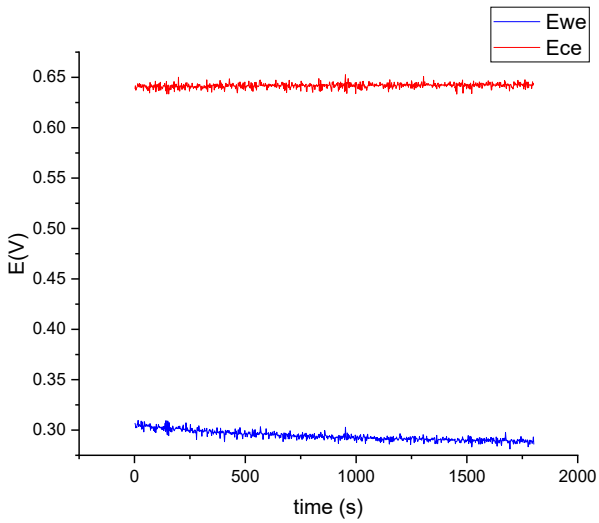

Figure 23: evolution in time of working and counter electrode potentials in OCV

3.3.2 Cyclic voltammetry (CV)

Cyclic voltammetry is an electrochemical technique performed by cycling the potential of the working electrode between two selected values and measuring the resulting current. The potential is measured between the working electrode and the reference electrode, while the current is measured between the working electrode and the counter electrode. The rate of voltage changes over time during each cycle is called scan rate. For this experiment, a CV consisting of 5 cycles between 0 and -2 V, at 10 mV/s was performed after the OCV. The following figure shows an example of the output of the CV, with the current on the Y-axis and the working electrode potential on the X-axis (Figure 24).

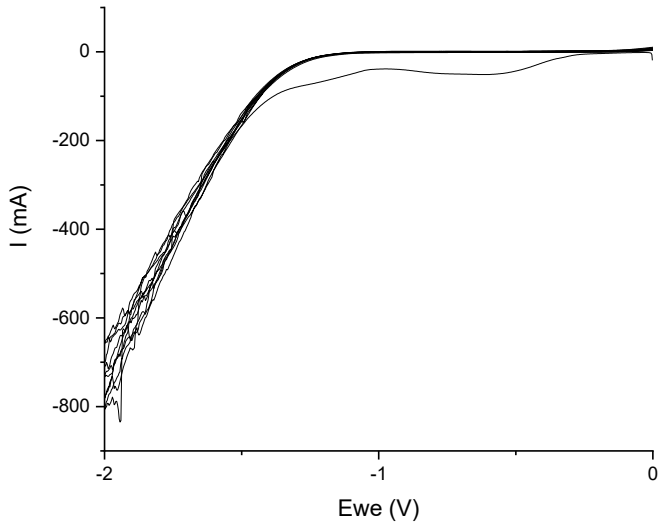

Figure 24: example of a Cyclic Voltammetry (CV)

3.3.3 Linear sweep voltammetry (LSV)

Linear sweep voltammetry is a method where the current between the working electrode and the counter electrode is measured while the potential between the working electrode and a reference electrode is swept linearly in time. The method

is similar to cyclic voltammetry, but rather than cycling over the potential range in both directions, linear sweep voltammetry involves only a single linear sweep from the lower potential limit to the upper potential limit. For this experiment, an LSV between 0 and -2 V, at 5 mV/s was performed after the CV. The following figure shows an example of the output of the LSV, with the current on the Y-axis and the working electrode potential on the X-axis (Figure 25).

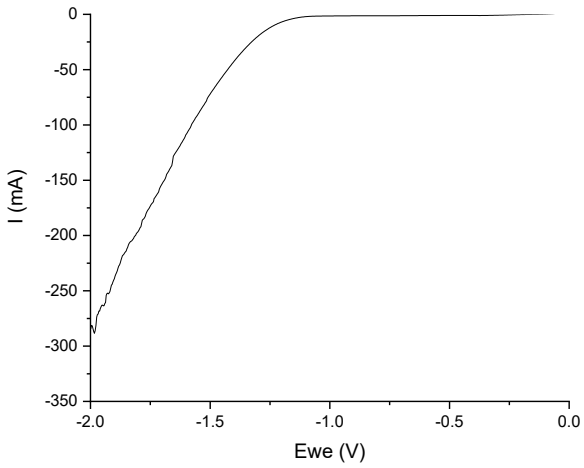

Figure 25: example of a Linear Sweep Voltammetry (LSV)

3.3.4 Chronoamperometry (CA)

Chronoamperometry is an electrochemical technique in which the variation of the current over time is measured while holding the potential of the working electrode constant. CA technique is used to measure the steady-state performance of an electrode at its operating potential. The desired potential to be applied during the CA should be a result of the previous CV test. For this experiment, a CA lasting 2 hours at -1.2 V was performed. The following figure shows an example of the output of the CA, with the time on the X-axis and the current on the Y-axis (Figure 26).

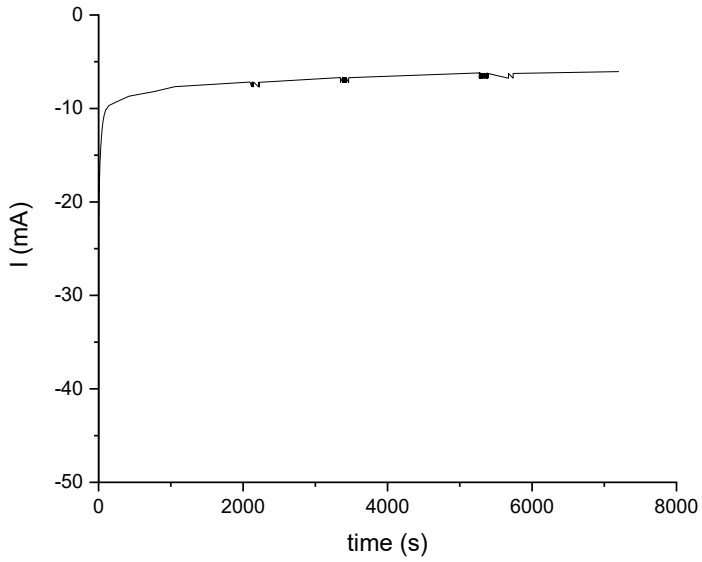

Figure 26: example of a Chronoamperometry (CA)

3.3.5 Chronopotentiometry (CP)

Chronopotentiometry is an electrochemical technique in which the variation of the working electrode potential over time is measured while holding the current constant. After several tests, CA was substituted by CP as the last technique of the protocol in order to keep the applied charge equal for all the tests and therefore increase the reproducibility. For this experiment, a CP lasting 2 hours at -8 mA was performed. The following figure shows an example of the output of the CP, with the time on the X-axis and the working electrode potential on the Y-axis (Figure 27).

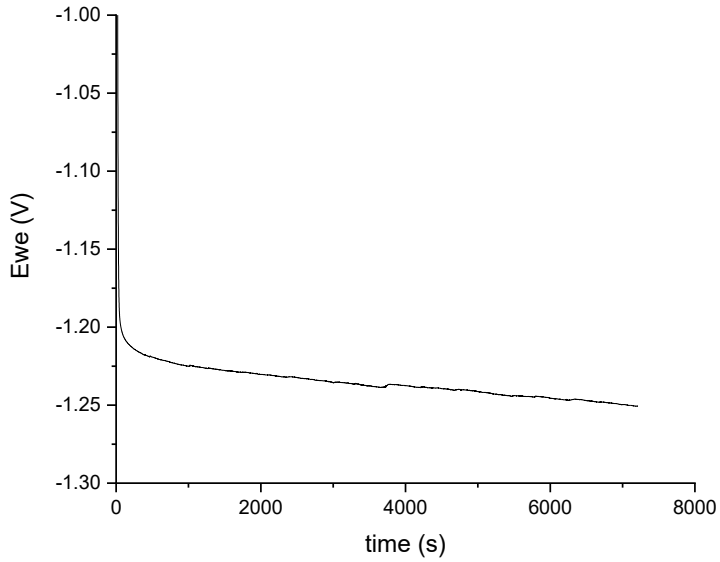

Figure 27: example of a chronopotentiometry (CP)

3.4 Analytical methods

For the performance evaluation of nitrate electroreduction, the quantification of reactants and products is needed. UV-vis spectroscopy is a convenient technique to quantify the ion concentration. If the ion has an absorption in UV-vis region (200-800 nm), a calibration curve can be made to quantify the ion concentration in solution. The samples collected before and after the CP/CA were analyzed to determine the concentration of NO_3^-, NO_2^- and NH_4^+. For that purpose, HITACHI U-5100 UV spectrophotometer was employed.

3.4.1 Spectrophotometry

A spectrophotometer is a device that is used to measure the amount of light absorbed by a sample at different wavelengths. It consists of a light source, a sample

holder, a diffraction prism to separate the light into different wavelengths, and a detector to measure the amount of light absorbed of each wavelength. The light source produces the photons that pass through the sample. The diffraction prism separates the light depending on the wavelength needed. The sample is held by a cuvette, that can be made of glass or quartz (depending on the wavelength needed). After the light passes through the sample, it travels to the detector that counts the number of photons reaching it. The collected data are plotted in the so-called absorption spectrum, where the wavelength is on the X-axis and the absorbance is on the Y-axis (Figure 28).

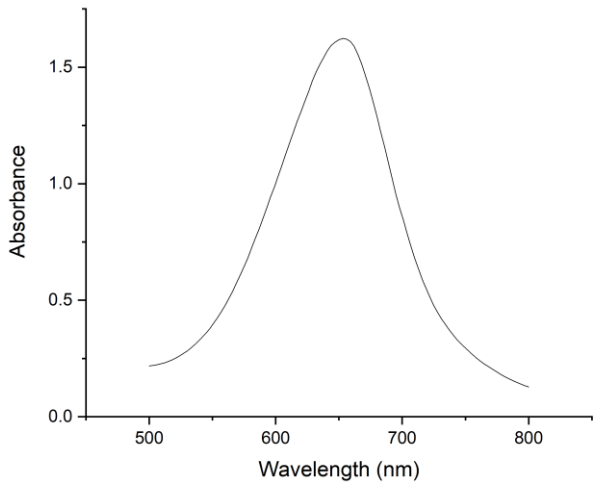

Figure 28: example of absorption spectrum

A calibration curve is used to determine the concentration of an unknown sample by comparing the unknown to a set of standard samples of known concentration. The absorbance of the samples of known concentration is measured using the spectrophotometer, and the data are plot with absorbance on the Y-axis and concentration on the X-axis. A statistical software is used to fit the data to a linear regression, giving as output the following equation:

$$y = mx + b \tag{3.6}$$

Where m is the slope, and b is the intercept of the curve (Figure 29). The coefficient of determination R^2 is the square of the correlation coefficient between actual and predicted y values. It quantifies the goodness of the fit, with 0 being the lower limit and 1 being the upper limit. A value of R^2 equal to 1 means that the fit is perfect.

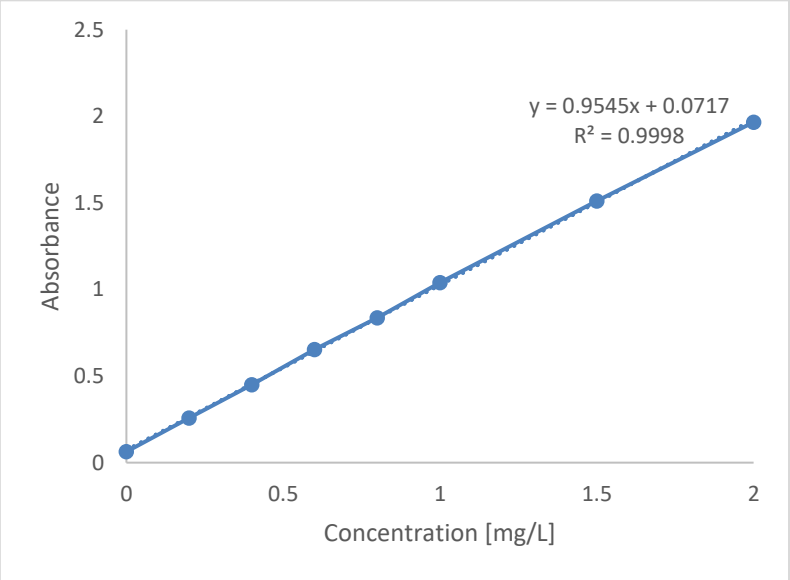

Figure 29: example of a calibration curve

3.4.2 Ammonia analysis

The concentration of NH_4^+ was determined spectrophotometrically by using the salicylate method based on the Berthelot reaction. The Berthelot reaction refers to a family of chemical reactions where a phenolic compound reacts with ammonia and a hypochlorite source to form an indophenol-like dye. [56] These indophenol-like dyes strongly absorb visible light between 630 nm and 720 nm, allowing for ammonia quantification using ultraviolet-visible spectroscopy. [23] The higher the

ammonia concentration, the bluer colored the dye will be (Figure 30). In the salicylate method, sodium salicylate is used as the phenolic compound, sodium hypochlorite is used as the hypochlorite source, and sodium nitroprusside is added as a catalyst. [57] The salicylate method has the advantage of avoiding toxic reagents but is sensitive to the color development time and the exposure to light, therefore the sample must be kept under dark for 45 minutes before analyzing it.

Figure 30: effect of ammonia concentration on the dye [58]

The salicylate method is the following: samples of 2 mL are added with 240 µL of salicylate catalyst solution (2.75 M $C_7H_5NaO_3$ and 0.95 mM $Na_2[Fe(CN)_5NO]\cdot 2H_2O$), followed by the addition of 400 µL of alkaline NaClO solution. After being kept under dark for 45 minutes, the absorbance at 650 nm of the samples is measured using the spectrophotometer. The concentration is determined according to the calibration lines obtained before. Then, the mass of NH_4^+ before and after the reaction is calculated as the product of the NH_4^+ concentration and the volume of the reservoir bottles (50 mL before and 46 mL after). Finally, the total produced ammonia is calculated as the difference between the mass of NH_4^+ after and before the reaction (considering both the anolyte and catholyte, and the acid trap).

3.4.3 Nitrates analysis

The concentration of NO_3^- was determined spectrophotometrically with the following method: samples of 5 mL are added with 100 µL of HCl 1 M to remove organic traces, followed by the addition of 10 µL of sulphanic acid (0.8% wt) to remove NO_2^-. [59] After 15 minutes, the absorbance at 220 nm and 275 nm is measured using the spectrophotometer. The absorbance of NO_3^- is obtained as follows:

$$A_{NO_3^-} = A_{220\,nm} - 2 \cdot A_{275\,nm} \tag{3.7}$$

The concentration is determined according to the calibration lines obtained before. Then, the mass of NO_3^- before and after the reaction is calculated as the product of the NO_3^- concentration and the volume of the reservoir bottles (50 mL before and 46 mL after). Finally, the total removed nitrates are calculated as the difference between the mass of NO_3^- after and before the reaction (considering both the anolyte and catholyte).

3.4.4 Nitrites analysis

There is no absorption for nitrite in the UV-vis range, thus the concentration of NO_2^- was determined spectrophotometrically by using the Griess method, which is based on the formation of a red-pink color dye after treatment of a sample with the Griess reagent (Figure 31). The Griess reagent consists of two components in an acidic solution: an aniline derivative and a coupling agent. The most common components are sulfanilamide and N-(1-naphthyl) ethylenediamine. The detection limit of the Griess test generally ranges between 0.02 and 2 µM, depending on the exact details of the components used in the Griess reagent. [60] The Griess method is the following: samples of 1 mL are added with 2 mL of water and 1 mL of Griess reagent. After 10 minutes, the absorbance at 540 nm is measured using the spectrophotometer. The concentration is determined according to the calibration

lines obtained before. Then, the mass of NO_2^- before and after the reaction is calculated as the product of the NO_2^- concentration and the volume of the reservoir bottles (50 mL before and 46 mL after). Finally, the total produced nitrites are calculated as the difference between the mass of NO_2^-after and before the reaction (considering both the anolyte and catholyte).

Figure 31: effect of nitrite concentration on the dye

3.4.5 Performance assessment

Faradaic efficiency (FE) and ammonia productivity (P) were used as figures of merit to assess the system performance. FE is defined as follows:

$$FE = \frac{n_x \cdot F \cdot n_{e^-}}{Q} \tag{3.8}$$

Where n_x is the produced moles of x, F is the Faraday's constant (equal to 96'485 C), n_{e^-} is the number of electrons needed to produce a mole of x (equal to 8 for the ammonia and 2 for the nitrites), and Q is the total charge applied. The NH_4^+ and NO_2^- considered for FE calculations are those produced during the CA or CP.
Ammonia productivity is defined as follows:

$$P = \frac{m_{NH_3}}{A \cdot t} \tag{3.9}$$

Where m_{NH_3} is the produced mass of ammonia, A is the electrode area, and t is the reaction time, expressed in hours. The reaction time for both CP and CA is equal to 2 hours.

Another parameter used to assess the system performance was the percentage of removed nitrates with respect to the initial nitrates present in the catholyte.

Chapter 4

4. Results and discussion

4.1 Cathode support selection

Three types of carbon paper with different characteristics have been tested to decide which one to use in the following tests as cathode support. The tested carbon papers were:

- Toray Paper 060
- N1S1007
- AVCarb MGL 190

K_2SO_4 0.3 M was added to both anolyte and catholyte to increase the conductivity, while 500 mg L^{-1} of nitrates were added only to catholyte, using KNO_3 as source. The system reached stability for all the tested supports after 30 minutes of OCV. From the CP and LSV it can be observed that the N1S1007 reached a much lower current density with respect to Toray Paper 060 and AvCarb MGL 190 (Figure 32). The worst performance was obtained using N1S1007, with a faradaic efficiency towards ammonia of 32%, while the Toray Paper 060 and AvCarb MGL 190 showed a better performance with values of 65.6% and 78.4% respectively. Considering the faradaic efficiency towards nitrites production, which should ideally be the lowest to increase the yield of ammonia, again the worst performance was observed when using N1S1007 as support, with a value of 17%. Toray Paper 060 and AvCarb MGL 190 showed a lower production of nitrites, resulting in values of faradaic efficiency of 7.1% and 6.8% respectively. The highest productivity was achieved using AvCarb MGL 190 as support (51.87 μg h^{-1} cm^{-2}), followed by Toray Paper 060 (43.58 μg h^{-1} cm^{-2}) and N1S1007 (8.74 μg h^{-1} cm^{-2}). Finally, the removed nitrates, calculated as percentage of the initial concentration

of nitrates, were 27.75% for Toray Paper 060, 12% for N1S1007 and 25.34% for AvCarb MGL 190.

Considering the better performance, AvCarb MGL 190 was the selected support for the following experiments.

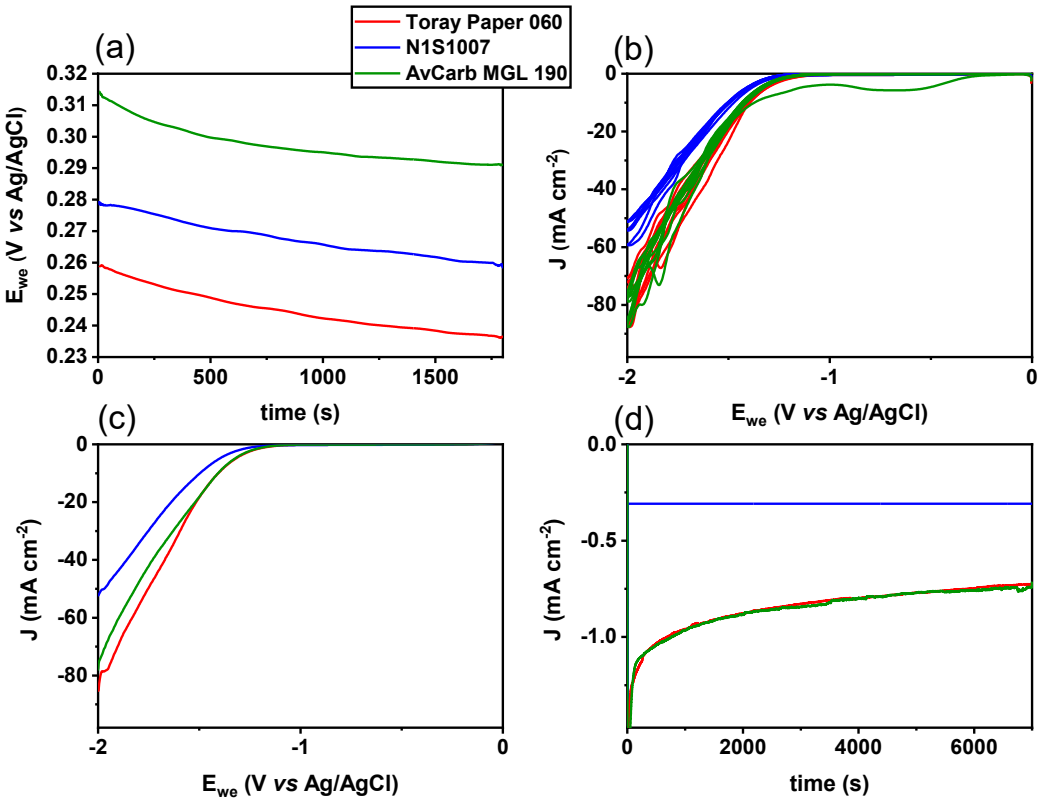

Figure 32: OCV (a), CV (b), LSV (c), CA (d) of Toray Paper 060, N1S1007 and AvCarb MGL 190

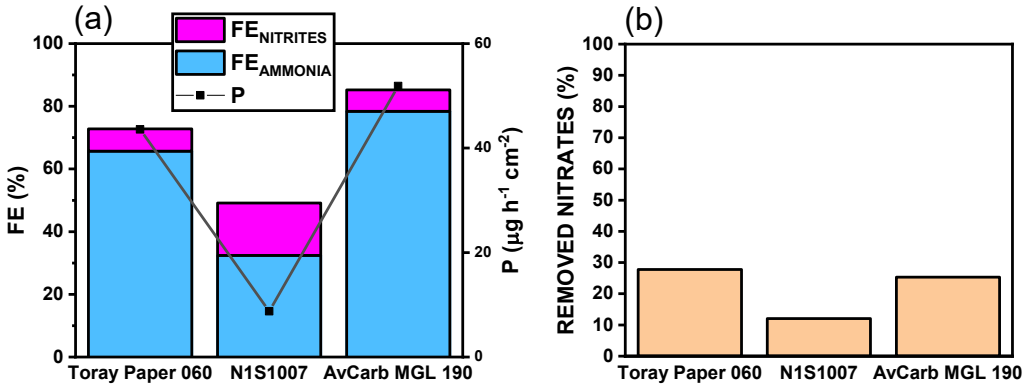

Figure 33: Faradaic efficiency and productivity (a), removed nitrates (b) of Toray Paper 060, N1S1007 and AvCarb MGL 190

4.2 Effect of the electrolyte composition

Different electrolytes have been tested to assess the impact of the supporting salt, its concentration and nitrate concentration in the process performance. In the first electrolyte tested, imitating real brackish water, Na_2SO_4 12.5 mM was added to both anolyte and catholyte, while a nitrate concentration of 2 mM was added only to the catholyte using $NaNO_3$ as source. The low salt and nitrate concentration led to the worst performances among all the electrolytes tested, with faradaic efficiency of 8.7% for ammonia and 2.8% for nitrites, productivity of 5.1 µg h^{-1} cm^{-2} and 25.8% of removed nitrates.

Then, in the second test, imitating real RO brine from brackish water, Na_2SO_4 concentration was increased up to 0.1 M, while also increasing nitrate concentration up to 6 mM. The results showed a huge increase in faradic efficiency (41.9% for

ammonia and 3% for nitrites) and in productivity (26 μg h^{-1} cm^{-2}), but a decrease in nitrate removal (18.4%).

In the third test, the effect of Na_2SO_4 concentration was studied; therefore, Na_2SO_4 was increased up to 0.3 M, while nitrate concentration was kept at 6 mM. The results showed an increase in faradaic efficiency (57.7% for ammonia and 2.4% for nitrites) and in productivity (35.9 μg h^{-1} cm^{-2}) with respect to the previous test.

In the last test, the effect of nitrate concentration was studied; in this case, Na_2SO_4 was kept fixed at 0.3 M, while nitrate concentration was increased up to 8 mM. The best performance was achieved with this electrolyte, with faradaic efficiency of 71.9% for ammonia and 5% for nitrites, productivity of 44.7 μg h^{-1} cm^{-2}. Analyzing the results obtained, it was observed that the initial nitrates concentration is a crucial parameter for their reduction. Increasing the initial nitrates concentration will increase the faradaic efficiency and ammonia productivity. The results showed also that salt concentration is another important parameter; considering the same initial nitrates concentration, using an electrolyte with higher salt concentration resulted in a better performance.

From the OCV it was observed that every configuration reached stability after 30' minutes. The CV and LSV showed that the configuration with Na_2SO_4 12.5 mM reached the lowest current density, while configurations with Na_2SO_4 0.3 M reached the highest one. This result was expected, considering that the presence of salt increases the conductivity of the electrolyte (Figure 34).

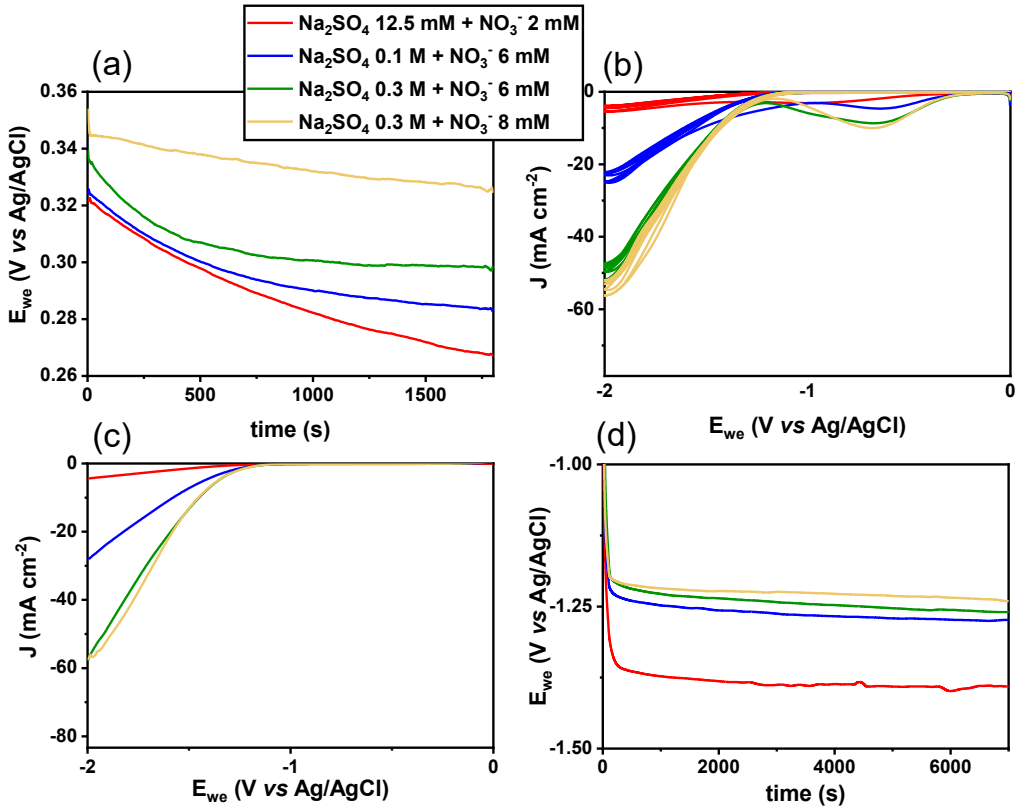

Figure 34: OCV (a), CV (b), LSV (c), CP (d) of the different electrolytes tested

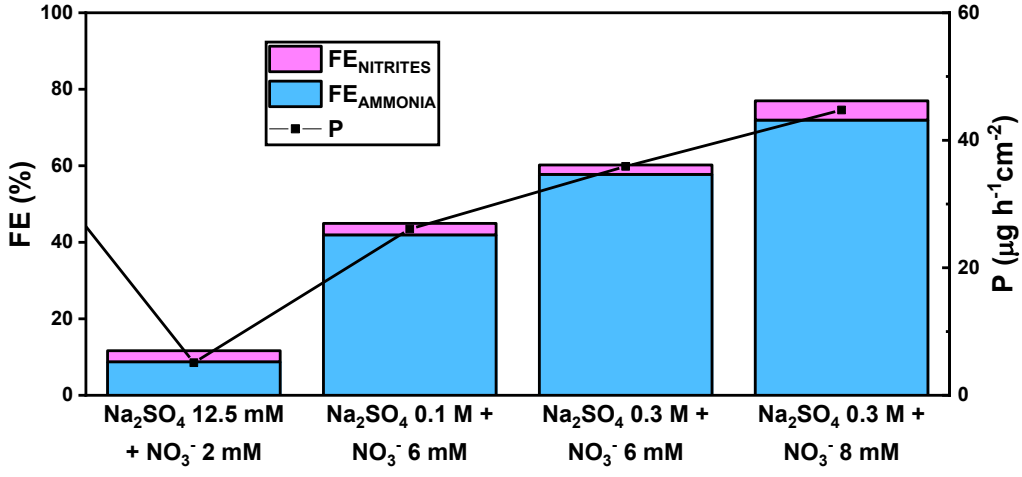

Figure 35: faradaic efficiency and productivity of the different electrolytes tested

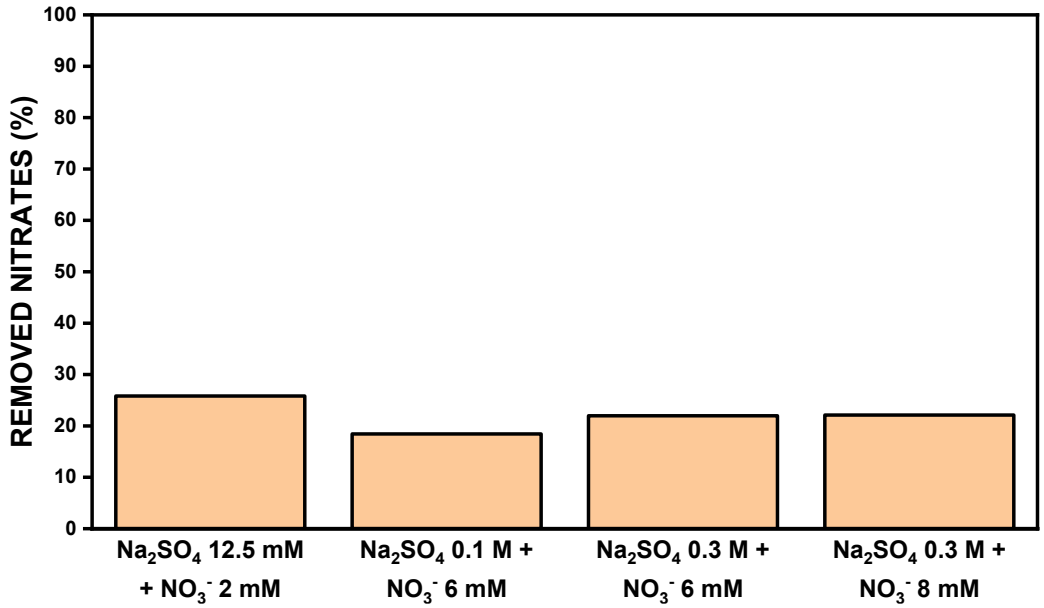

Figure 36: removed nitrates of the different electrolytes tested

4.2.1 Na_2SO_4 vs K_2SO_4

The obtained results demonstrated the necessity of a configuration with salt concentration of 0.3 M and nitrate concentration of 8 mM to achieve the best performance in nitrate removal while still maintaining concentrations similar to those found in real water sources. Overall, the configuration with K_2SO_4 showed better performance in every aspect of the analysis compared to Na_2SO_4. However, the difference is minimal, and sodium is more present than potassium in real water. The use of sodium allows for a more accurate study of electrochemical reduction in real-world conditions, enabling the analysis of the effects of various elements present in real water, which can be added as sodium compounds to the electrolyte. For these reasons, Na_2SO_4 0.3 M and NO_3^- 8 mM were selected as model electrolyte.

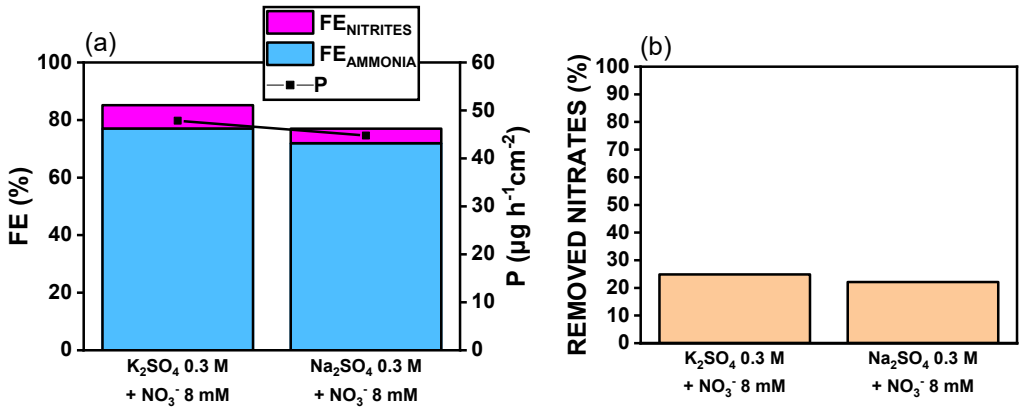

Figure 37: faradaic efficiency and productivity (a), removed nitrates (b) of K_2SO_4 and Na_2SO_4

4.3 Influence of water elements on nitrate electroreduction reaction

Starting from the "optimum" electrolyte selected before (Na_2SO_4 0.3 M + NO_3^- 8 mM), the analysis of a simulated brackish groundwater RO brine was performed considering firstly the single effect of different elements presents in the water, and then the combined effect of these elements to simulate a real water condition.

4.3.1 Mg^{2+}

157 mg L^{-1} of Mg^{2+} were added to both catholyte and anolyte, using $MgSO_4$ as the source. The results were compared with the case without Mg^{2+}. The presence of the $MgSO_4$ increased the conductivity of the electrolyte, resulting in higher current reached during CV and LSV, and lower working electrode potential during CP (Figure 38). Despite this, the performance was much lower, with a faradaic efficiency of 45.2% (39.6% towards ammonia and 5.6% towards nitrites), ammonia productivity of 24.64 μg h^{-1} cm^{-2} and 18.17% of removed nitrates. Furthermore, a

white layer above the electrode was observed, and it persisted even after rising with water (Figure 39), meaning that Mg^{2+} probably poisoned the electrodes and thus reduced the efficiency of the system.

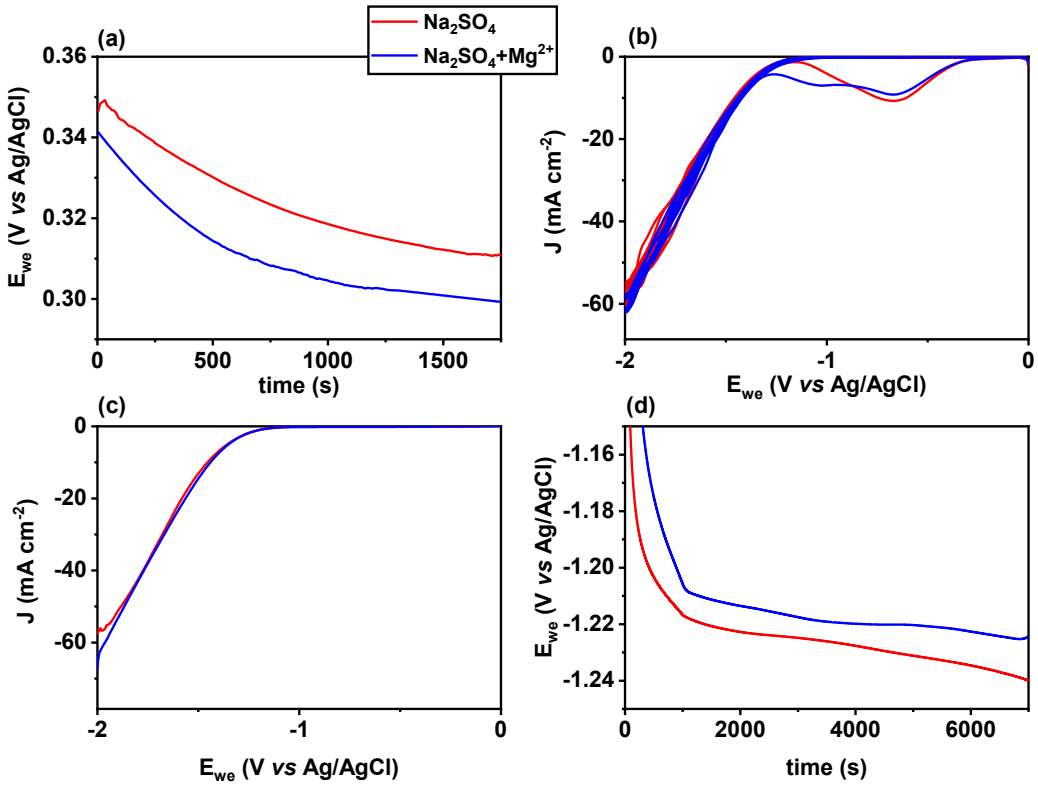

Figure 38: Effect of Mg^{2+} on OCV (a), CV (b), LSV (c), CP (d)

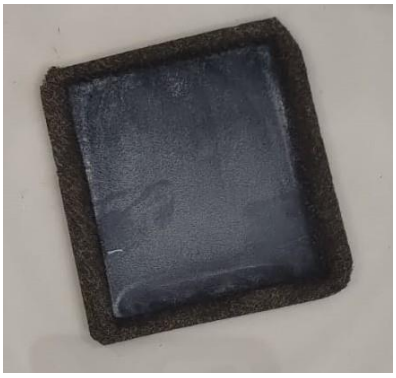

Figure 39: carbon paper after magnesium precipitation

4.3.2 HCO_3^-

417 mg L^{-1} of HCO_3^- were added to both catholyte and anolyte, using $NaHCO_3$ as the source. The presence of $NaHCO_3$ increased the conductivity of the electrolyte, resulting in higher current reached during CV and LSV (Figure 40). The presence of HCO_3^- significantly increased the performance; faradaic efficiency increased up to 83.6% (76.4% towards ammonia and 7.2% towards nitrites), ammonia productivity increased up to 47.53 µg h^{-1} cm^{-2} and nitrated removed increased up to 26%.

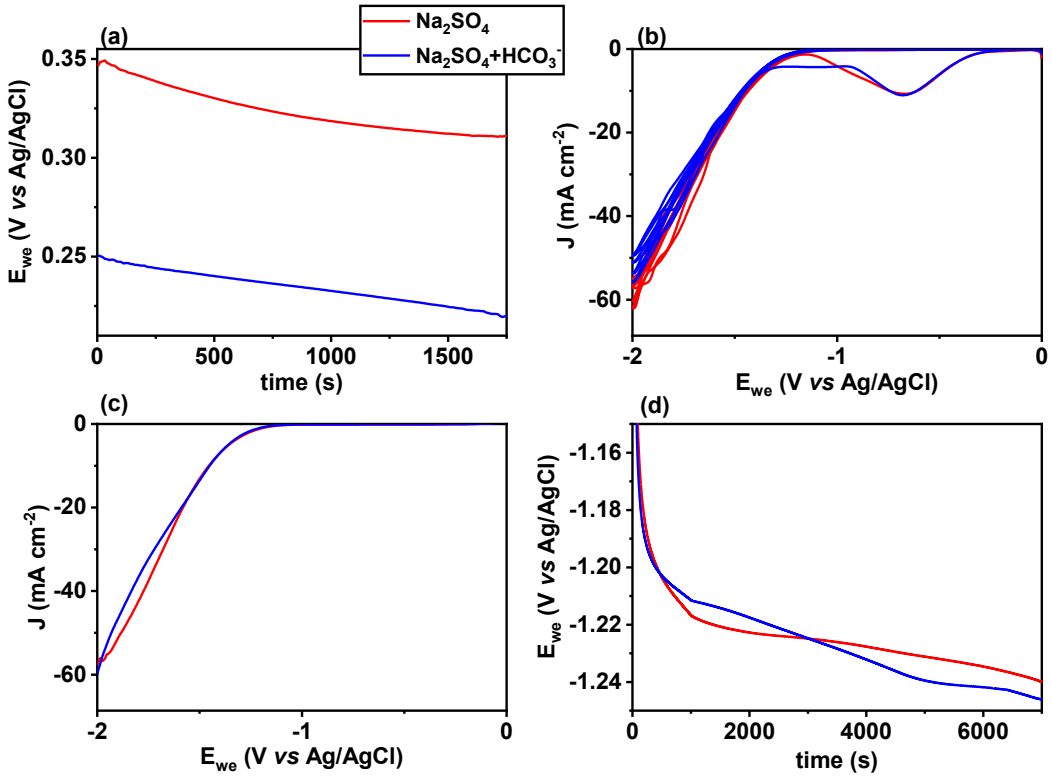

Figure 40: Effect of HCO_3^- on OCV (a), CV (b), LSV (c), CP (d)

4.3.3 F^-

4 mg L^{-1} of F^- were added to both catholyte and anolyte, using NaF as the source. The added quantity was so small that the electrolyte conductivity was not significantly influenced in comparison with the case without F^-, and so CV, LSV and CP did not show variations (Figure 41). The presence of F^- slightly reduced both ammonia faradaic efficiency and productivity, with the former going from 71.9% to 70.5%, and the latter going from 44.7 µg h^{-1} cm^{-2} to 43.8 µg h^{-1} cm^{-2}. Nitrite faradaic efficiency increased up to 5.5% due the presence of F^-, while removed nitrates increased up to 24.6%. Anyway, the effect of F^- can be considered as negligible.

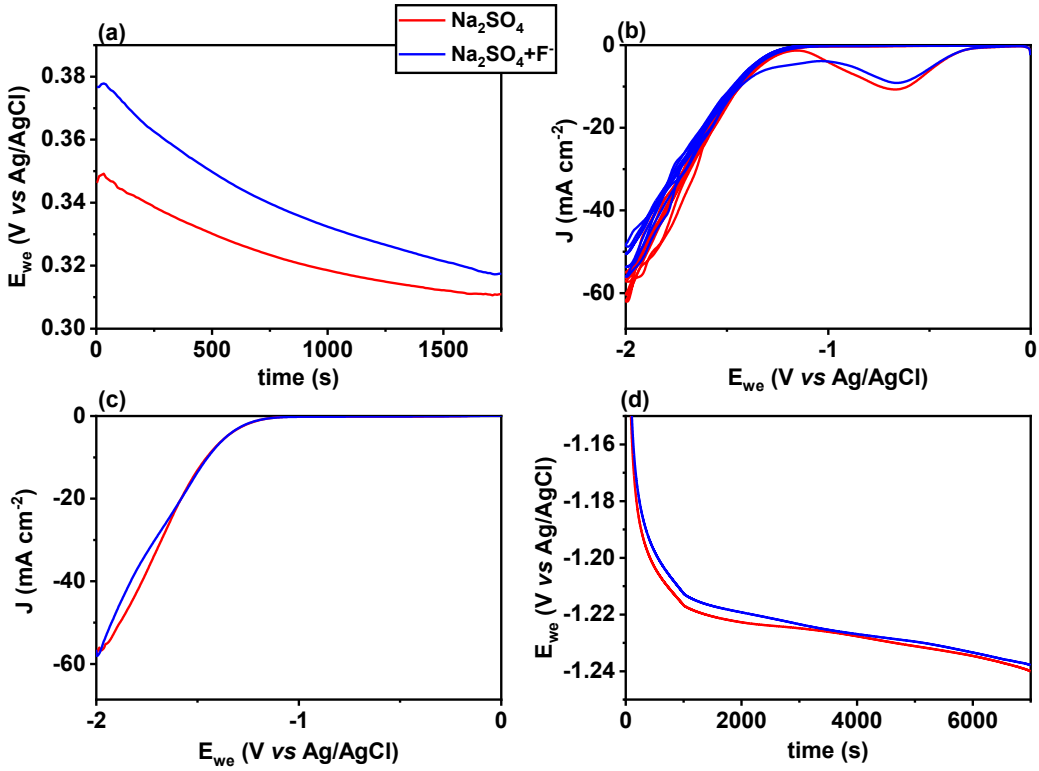

Figure 41: Effect of F^- on OCV (a), CV (b), LSV (c), CP (d)

4.3.4 Cl^-

5522 mg L^{-1} of Cl^- were added to both catholyte and anolyte, using NaCl as the source. The results were compared with the case without Cl^-. The presence of a large quantity of NaCl increased the conductivity of the electrolyte, resulting in higher current reached during CV and LSV (Figure 42). The presence of Cl^- decreased the performance; faradaic efficiency decreased up to 62.2% towards ammonia and increased up to 7.1% towards nitrites, ammonia productivity decreased up to 38.68 µg h^{-1} cm^{-2} and nitrated removed decreased up to 21%.

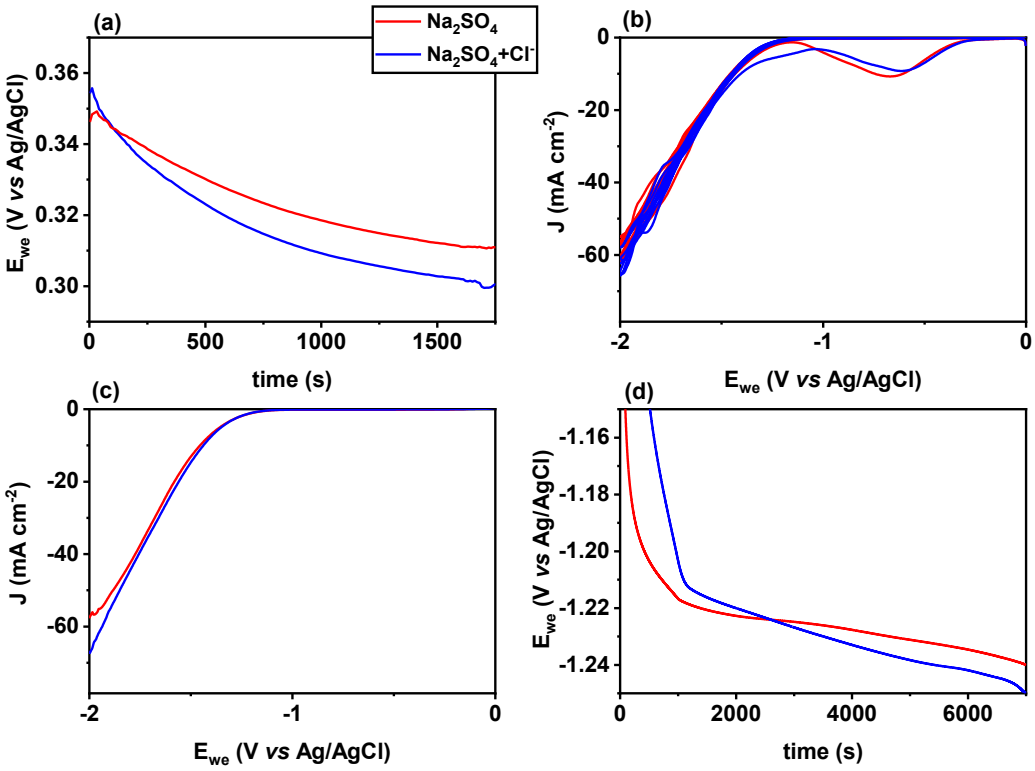

Figure 42: Effect of Cl^- on OCV (a), CV (b), LSV (c), CP (d)

4.3.5 K^+

74 mg L^{-1} of K^+ were added to both catholyte and anolyte, using K_2SO_4 as the source. The results were compared with the case without K^+. The presence of K_2SO_4 increased the conductivity of the electrolyte, resulting in higher current being reached during CV and LSV (Figure 43). Opposite to what was expected, the presence of K^+ slightly decreased the performance; faradaic efficiency decreased up to 70.4% towards ammonia and increased up to 7.3% towards nitrites, ammonia productivity decreased up to 43.78 µg h^{-1} cm^{-2} and nitrated removed decreased up to 22%.

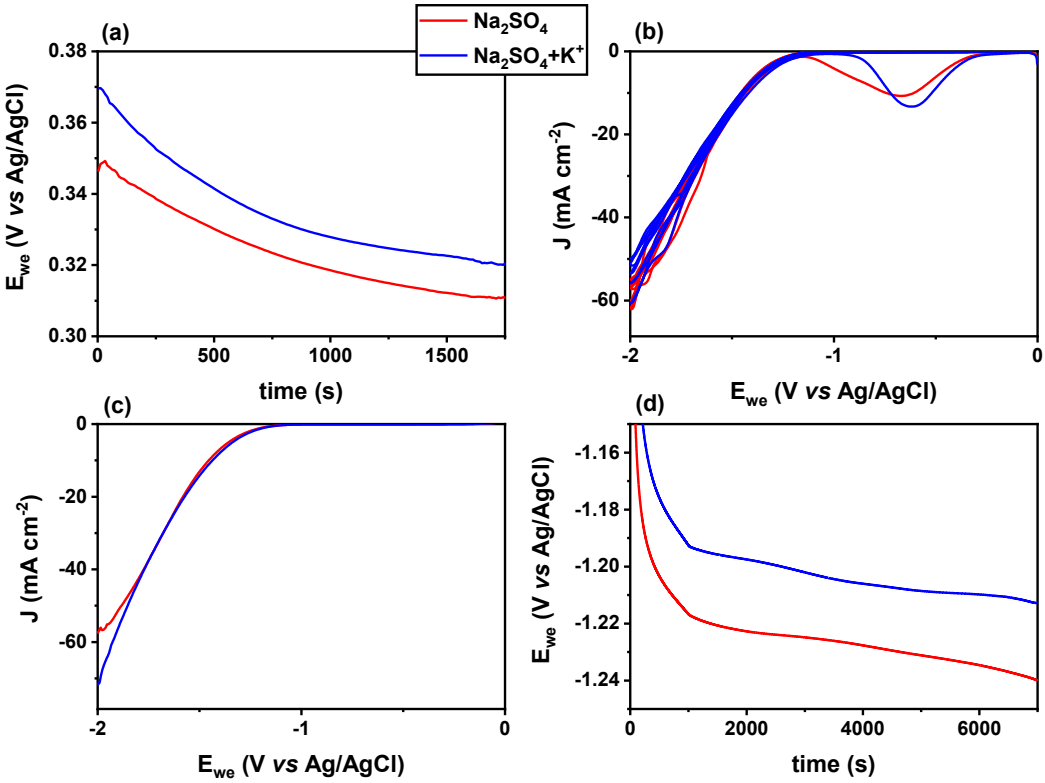

Figure 43: Effect of K^+ on OCV (a), CV (b), LSV (c), CP (d)

4.3.6 PO_4^{3-}

0.4 mg L^{-1} of PO_4^{3-} were added to both catholyte and anolyte, using NaH_2PO_4 as the source. The results were compared with the case without PO_4^{3-}. The presence of NaH_2PO_4 did not affect the conductivity of the electrolyte, resulting in a similar current being reached during CV and LSV (Figure 44). The presence of PO_4^{3-} slightly decreased the performance; faradaic efficiency decreased up to 70.4% towards ammonia and increased up to 6.2% towards nitrites, ammonia productivity decreased up to 43.81 µg h^{-1} cm^{-2} and nitrated removed decreased up to 21.4%.

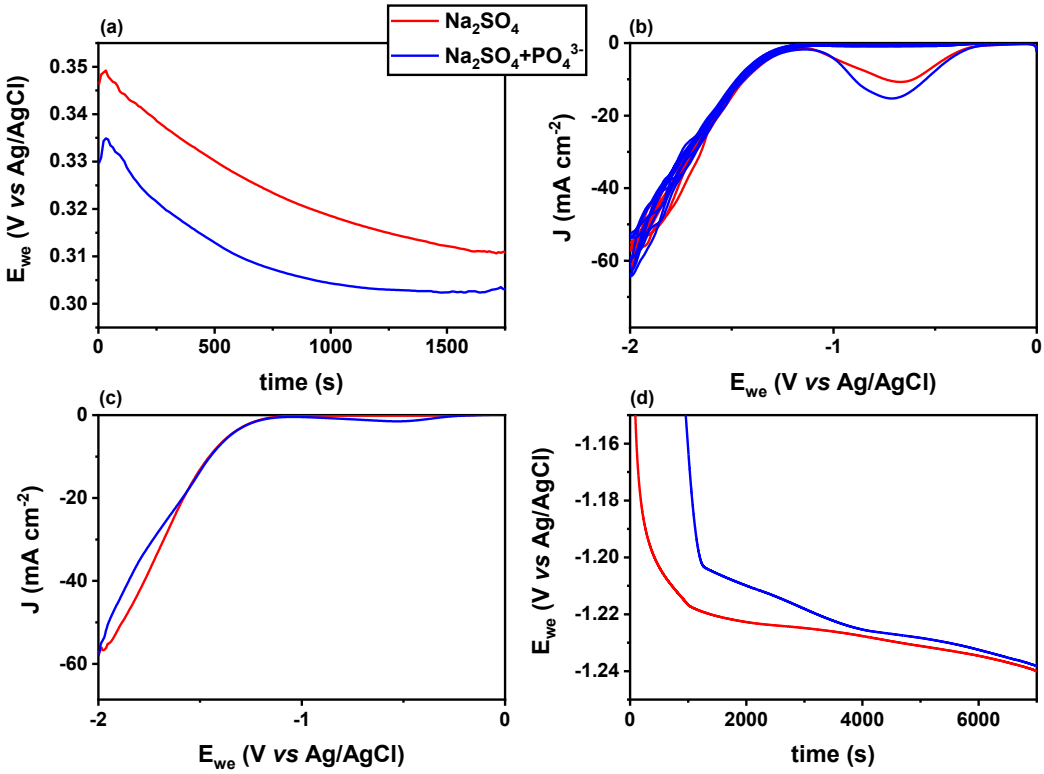

Figure 44: Effect of PO_4^{3-} on OCV (a), CV (b), LSV (c), CP (d)

4.3.7 SiO_2

50 mg L^{-1} of SiO_2 were added to both catholyte and anolyte, using Na_2SiO_3 as the source. The results were compared with the case without SiO_2. The presence of Na_2SiO_3 did not affect the conductivity of the electrolyte, slightly increasing the current being reached during CV and LSV (Figure 45). The presence of SiO_2 slightly increased the performance; faradaic efficiency increased up to 72.3% towards ammonia and increased up to 9% towards nitrites, ammonia productivity increased up to 44.94 μg h^{-1} cm^{-2} and nitrated removed increased up to 23.5%.

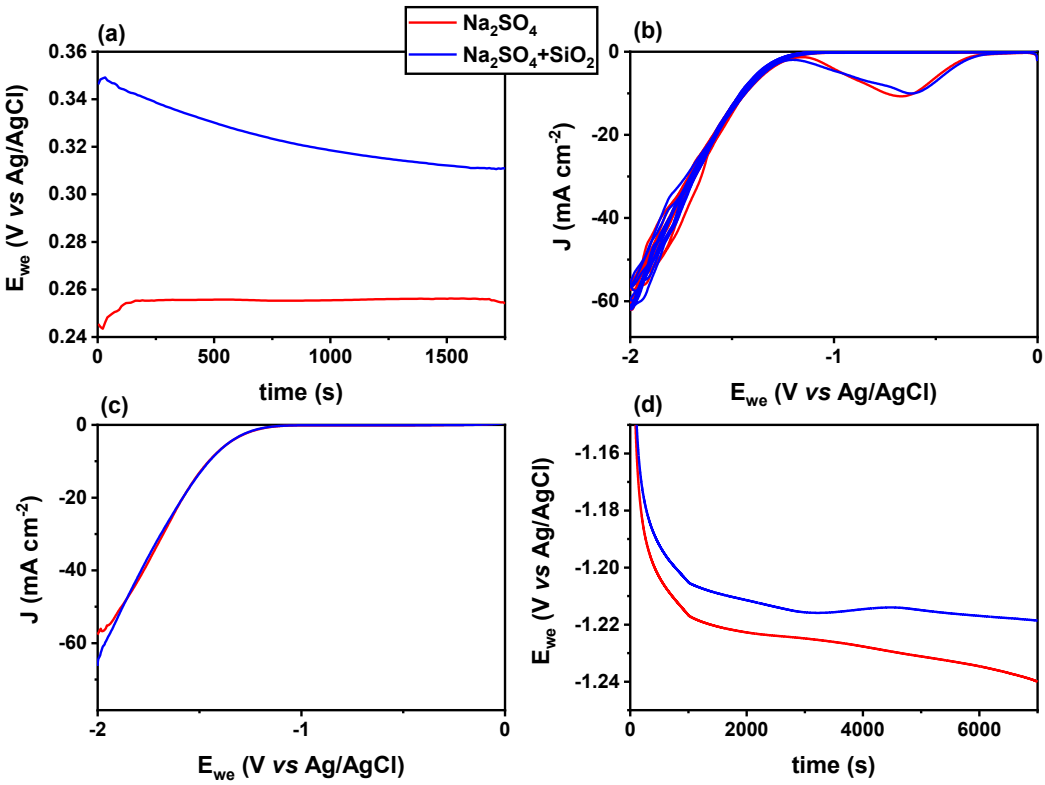

Figure 45: Effect of SiO_2 on OCV (a), CV (b), LSV (c), CP (d)

4.3.8 Humic acids

4 mg L^{-1} of humic acids (HA) were added to both catholyte and anolyte. The results were compared with the case without HA. The presence of HA reduced the conductivity of the electrolyte, resulting in a reduced current being reached during CV and LSV (Figure 46), and decreased the performance; faradaic efficiency decreased up to 62% towards ammonia and increased up to 6.8% towards nitrites, ammonia productivity decreased up to 38.55 µg h^{-1} cm^{-2} and nitrated removed decreased up to 21.6%.

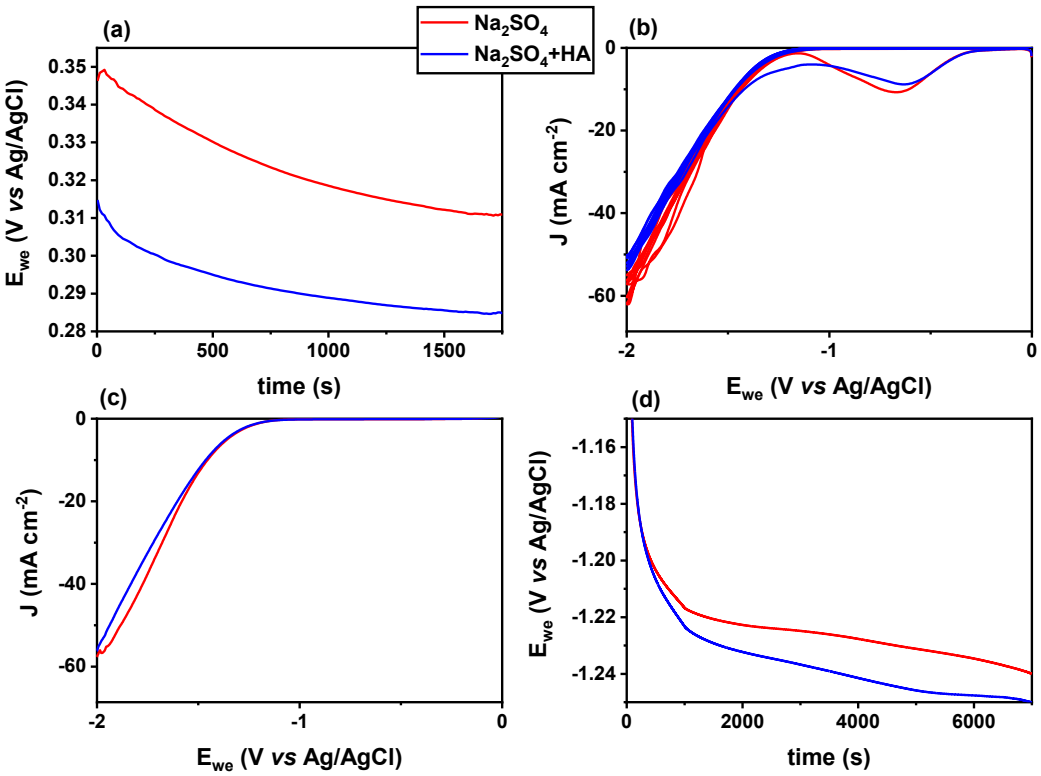

Figure 46: Effect of HA on OCV (a), CV (b), LSV (c), CP (d)

4.3.9 Ca^{2+}

567 mg L^{-1} of Ca^{2+} were added to both catholyte and anolyte, using $CaCl_2$ as the source. The presence of Ca^{2+} did not significantly influence the conductivity of the electrolyte, leading to similar current reached during CV and LSV in contrast to the case without the calcium (Figure 47). However, the performance of the system was strongly reduced: faradaic efficiency was reduced up to 47.7% towards ammonia and up to 4.39% towards nitrites, productivity was decreased up to 29.67 µg h^{-1} cm^{-2} and removed nitrates were decreased up to 18.51%.

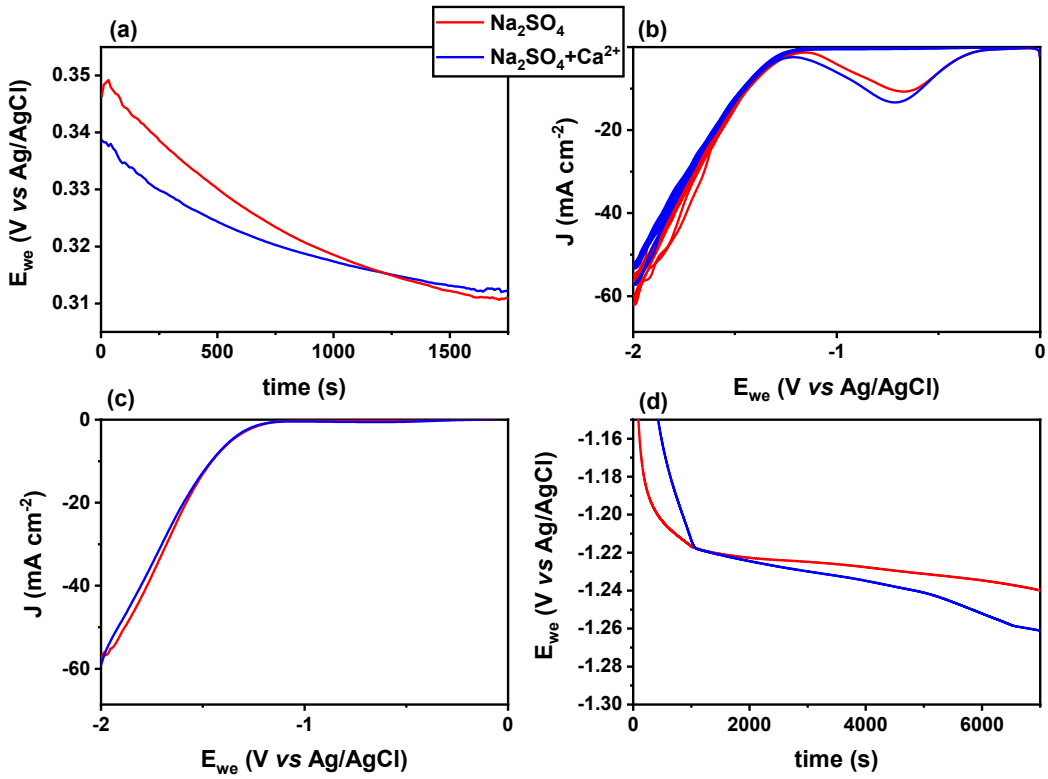

Figure 47: Effect of Ca^{2+} on OCV (a), CV (b), LSV (c), CP (d)

4.3.10 Simulated water

Two tests of simulated water containing all the previous elements were performed. The first was performed without the presence of Na_2SO_4 0.3 M as supporting salt in the electrolyte, to simulate more accurately real water conditions. The absence of the salt led to much lower currents being reached during CV and LSV. The performance was drastically reduced: faradaic efficiency drop of to 9.6% towards ammonia and the productivity was reduced to 5.96 μg h^{-1} cm^{-2}. Then, a second test was performed, adding Na_2SO_4 0.3 M as supporting salt to study whether it has a positive effect or not. The presence of the salt led in this case to higher currents being reached during CV and LSV (Figure 48). Despite the higher currents, the presence of all the elements negatively affected the performance of the system: faradaic efficiency was reduced to 26.7% while ammonia productivity was reduced to 16.6 μg h^{-1} cm^{-2}.

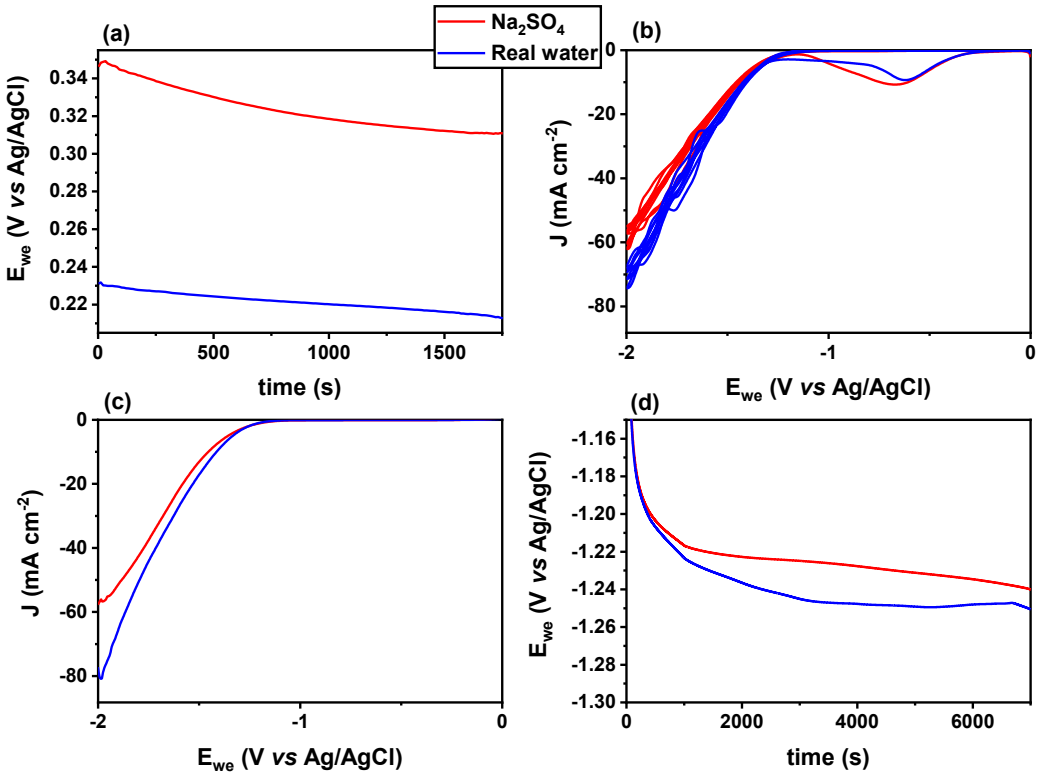

Figure 48: Effect of all the elements on OCV (a), CV (b), LSV (c), CP (d)

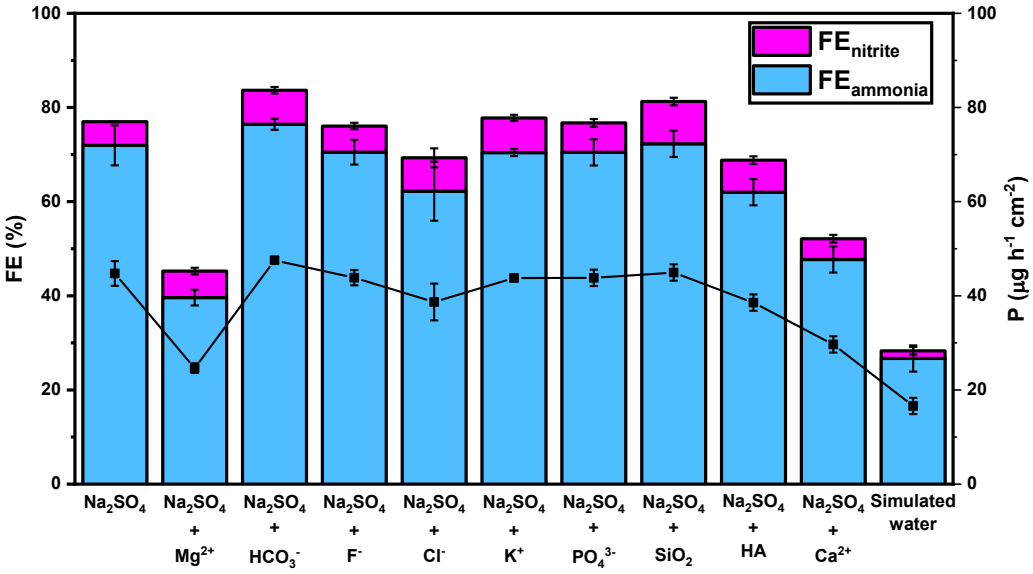

Figure 49: Effect of the elements on faradaic efficiency and productivity

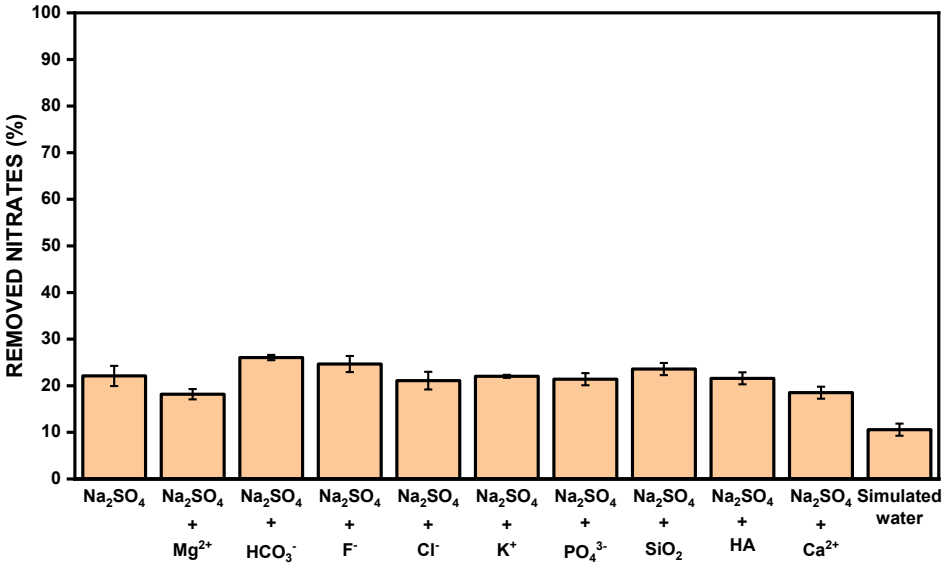

Figure 50: Effect of the elements on nitrate removal

The summary of the results is showed in Table 7. The configuration which showed the best overall performance was the one with 0.3 M K_2SO_4 as supporting salt in

the electrolyte. Good results were also obtained by using 0.3 M Na_2SO_4. The presence of different elements in the electrolyte affected the results in different ways. Considering the single elements, the worst performances of the system was obtained in presence of Mg^{2+} and Ca^{2+}. Other elements like Cl^- and HA slightly decreased the performance of the system, while the effect of elements like F^-, K^+ and PO_4^{3-} was negligible. On the other hand, the presence in the electrolyte of HCO_3^- and SiO_2 led to an increase of the system performance. In particular, the best performance of the system was obtained in presence of HCO_3^-, resulting in the highest faradaic efficiency and nitrate removal. However, the simultaneous presence of all these elements drastically reduced the performance of the system, and the lowest values of faradaic efficiency and nitrate removal were observed in the case of simulated water. The values of pH measured in both anolyte and catholyte after the CP is shown in Figure 51. The pH at the catholyte oscillates between 10.5 and 12, while at the anolyte between 2.5 and 2.8.

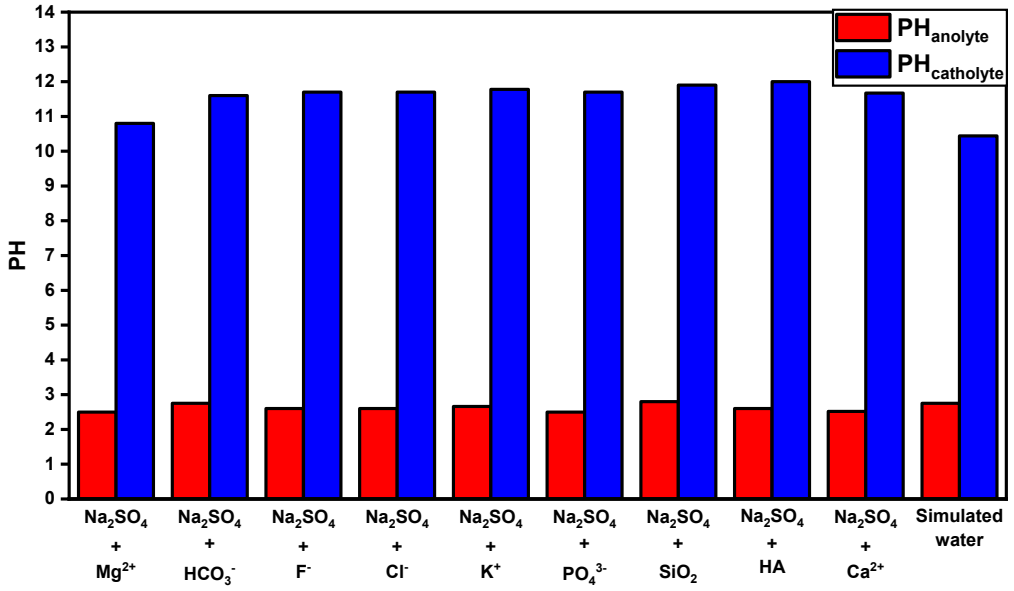

Figure 51: Effect of the elements on pH

	Ammonia faradaic efficiency (%)	***Ammonia productivity ($\mu g\ h^{-1}\ cm^{-2}$)***	***Nitrite faradaic efficiency (%)***	***Removed nitrates (%)***
Na_2SO_4 0.3 M	71.95	44.74	5.02	22.10
Na_2SO_4 0.3 M + Mg^{2+}	39.63	24.64	5.61	18.17
Na_2SO_4 0.3 M + HCO_3^-	76.44	47.53	7.20	26.04
Na_2SO_4 0.3 M + F^-	70.50	43.84	5.55	24.65
Na_2SO_4 0.3 M + Cl^-	62.20	38.68	7.10	21.09
Na_2SO_4 0.3 M + K^+	70.41	43.78	7.35	22.02
Na_2SO_4 0.3 M + PO_4^{3-}	70.46	43.81	6.26	21.42
Na_2SO_4 0.3 M + SiO_2	72.28	44.94	8.98	23.57
Na_2SO_4 0.3 M + HA	62.00	38.55	6.81	21.59
Na_2SO_4 0.3 M + Ca^{2+}	47.72	29.67	4.39	18.51
Simulated water	26.69	16.60	1.62	10.57
K_2SO_4 0.3 M	77.04	47.86	8.08	24.88

Table 7: Summary of result

Conclusion

This work explores the impact of the anions/cations present in brackish groundwater RO brines on the electrochemical reduction of nitrate. It was observed that the presence of different elements in water can affect the performance of electrochemical nitrate reduction. Some elements, such as HCO_3^-, K^+ and SiO_2, increased the performance, while other elements, such as Mg^{2+}, F^-, HA and Ca^{2+}, decreased the performance of the system. The simultaneous presence of all these elments in water drastically decreased system performance, with faradaic efficiency going from 71.9% to 26.7% and productivity going from 44.74 μg h^{-1} cm^{-2} to 16.6 μg h^{-1} cm^{-2}. The drastic loss in performance was attributed mainly to inorganic scaling formation on the cathode surface. The formation of these precipitates decreased the efficiency of the process by creating a physical barrier, which makes the electron transfer at the electrode surface difficult. The obtained results show that it is possible to carry out the electrochemical nitrate reduction of brackish groundwater RO brine with decent efficiency. However, further development and better understanding of the phenomena are needed to reach a full-scale application.

Bibliography

[1] A. Richa, S. Touil, e M. Fizir, «Recent advances in the source identification and remediation techniques of nitrate contaminated groundwater: A review», *Journal of Environmental Management*, vol. 316, p. 115265, ago. 2022, doi: 10.1016/j.jenvman.2022.115265.

[2] «Appendix 3 FAO Irrigation Water Quality Guidelines», in *Water Wells and Boreholes*, John Wiley & Sons, Ltd, 2006, pp. 469–470. doi: 10.1002/0470031344.app3.

[3] N. N. Greenwood e A. Earnshaw, A c. di, «11 - Nitrogen», in *Chemistry of the Elements (Second Edition)*, Oxford: Butterworth-Heinemann, 1997, pp. 406–472. doi: 10.1016/B978-0-7506-3365-9.50017-1.

[4] P. M. Vitousek *et al.*, «Human Alteration of the Global Nitrogen Cycle: Sources and Consequences», *Ecological Applications*, vol. 7, fasc. 3, pp. 737–750, 1997, doi: 10.1890/1051-0761(1997)007[0737:HAOTGN]2.0.CO;2.

[5] J. A. Fernández-López, M. Alacid, J. M. Obón, R. Martínez-Vives, e J. M. Angosto, «Nitrate-Polluted Waterbodies Remediation: Global Insights into Treatments for Compliance», *Applied Sciences*, vol. 13, fasc. 7, Art. fasc. 7, gen. 2023, doi: 10.3390/app13074154.

[6] M. H. Ward *et al.*, «Drinking Water Nitrate and Human Health: An Updated Review», *Int J Environ Res Public Health*, vol. 15, fasc. 7, p. 1557, lug. 2018, doi: 10.3390/ijerph15071557.

[7] «Directive - 2020/2184 - EN - EUR-Lex». Consultato: 14 febbraio 2025. [Online]. Disponibile su: https://eur-lex.europa.eu/eli/dir/2020/2184/oj/eng

[8] *Directive 2006/118/EC of the European Parliament and of the Council of 12 December 2006 on the protection of groundwater against pollution and deterioration*, vol. 372. 2006. Consultato: 14 febbraio 2025. [Online]. Disponibile su: http://data.europa.eu/eli/dir/2006/118/oj/eng

[9] «Nitrates Directive - Reporting 7». Consultato: 20 dicembre 2024. [Online]. Disponibile su: https://water.jrc.ec.europa.eu/portal/apps/dashboards/cb6034c2a75e4df282f8a62f90c16caa%20

[10] «Nitrate in groundwater in Europe». Consultato: 14 febbraio 2025. [Online]. Disponibile su: https://www.eea.europa.eu/en/analysis/indicators/nitrate-in-groundwater-8th-eap

[11] «Waterbase - Water Quality ICM». Consultato: 14 febbraio 2025. [Online]. Disponibile su: https://www.eea.europa.eu/en/datahub/datahubitem-view/fbf3717c-cd7b-4785-933a-d0cf510542e1?activeAccordion=1092907

[12] S. Jiang, Y. Li, e B. P. Ladewig, «A review of reverse osmosis membrane fouling and control strategies», *Science of The Total Environment*, vol. 595, pp. 567–583, ott. 2017, doi: 10.1016/j.scitotenv.2017.03.235.

[13] «(PDF) Systems for ammonium concentration for further removal in the partial nitritation/anammox technology», ResearchGate. Consultato: 18 febbraio 2025. [Online]. Disponibile su: https://www.researchgate.net/publication/262794103_Systems_for_ammonium_concentration_for_further_removal_in_the_partial_nitritationanammox_technology

[14] U. E. N. C. for E. Assessment, «Biological denitrification of high nitrate water: Influence of type of carbon source and nitrate loading». Consultato: 18 febbraio 2025. [Online]. Disponibile su: https://hero.epa.gov/hero/index.cfm/reference/details/reference_id/1190683

[15] «Executive Summary – Ammonia Technology Roadmap – Analysis», IEA. Consultato: 9 febbraio 2025. [Online]. Disponibile su: https://www.iea.org/reports/ammonia-technology-roadmap/executive-summary

[16] «Enriching the Earth. Fritz Haber, Carl Bosch, and the Transformation of World Food Production», *ResearchGate*, nov. 2024, doi: 10.2307/3985938.

[17] R. Lan, J. T. S. Irvine, e S. Tao, «Synthesis of ammonia directly from air and water at ambient temperature and pressure», *Sci Rep*, vol. 3, fasc. 1, p. 1145, gen. 2013, doi: 10.1038/srep01145.

[18] «Introduction to Ammonia Production». Consultato: 23 dicembre 2024. [Online]. Disponibile su: https://www.aiche.org/resources/publications/cep/2016/september/introduction-ammonia-production

[19] «The Haber Process», Chemistry LibreTexts. Consultato: 23 dicembre 2024. [Online]. Disponibile su: https://chem.libretexts.org/Bookshelves/Physical_and_Theoretical_Chemistry_Textbook_Maps/Supplemental_Modules_(Physical_and_Theoretical_Chemistry)/Equilibria/Le_Chateliers_Principle/The_Haber_Process

[20] J. G. Speight, *The refinery of the future*, 2nd ed. Cambridge, MA: Gulf Professional Publishing, 2020. Consultato: 9 febbraio 2025. [Online]. Disponibile su: https://search.ebscohost.com/login.aspx?direct=true&scope=site&db=nlebk&db=nlabk&AN=2367421

[21] A. O. Gezerman, «A Critical Assessment of Green Ammonia Production and Ammonia Production Technologies», *Kemija u industriji*, fasc. 1–2, gen. 2022, doi: 10.15255/KUI.2021.013.

[22] L. University, «Electrochemically-produced ammonia could revolutionize food production». Consultato: 9 febbraio 2025. [Online]. Disponibile su: https://phys.org/news/2018-07-electrochemically-produced-ammonia-revolutionize-food-production.html

[23] Y. Song *et al.*, «A physical catalyst for the electrolysis of nitrogen to ammonia», *Science Advances*, vol. 4, fasc. 4, p. e1700336, apr. 2018, doi: 10.1126/sciadv.1700336.

[24] «(PDF) DYNAMICS OF AMMONIA SYNTHESIS FROM INDUSTRIAL REACTORS: A GAZE TOWARDS PRODUCTION DIVERSITY», in *ResearchGate*, Consultato: 17 febbraio 2025. [Online]. Disponibile su:

https://www.researchgate.net/publication/380124128_DYNAMICS_OF_AMMONIA_SYNTHESIS_FROM_INDUSTRIAL_REACTORS_A_GAZE_TOWARDS_PRODUCTION_DIVERSITY

[25] H. Zhang *et al.*, «Strategies and applications of electrocatalytic nitrate reduction towards ammonia», *Coordination Chemistry Reviews*, vol. 506, p. 215723, mag. 2024, doi: 10.1016/j.ccr.2024.215723.

[26] T. Wu, W. Fan, Y. Zhang, e F. Zhang, «Electrochemical synthesis of ammonia: Progress and challenges», *Materials Today Physics*, vol. 16, p. 100310, gen. 2021, doi: 10.1016/j.mtphys.2020.100310.

[27] H. Xu, Y. Ma, J. Chen, W. Zhang, e J. Yang, «Electrocatalytic reduction of nitrate – a step towards a sustainable nitrogen cycle», *Chem. Soc. Rev.*, vol. 51, fasc. 7, pp. 2710–2758, apr. 2022, doi: 10.1039/D1CS00857A.

[28] «The role of energy storage tech in the energy transition», World Economic Forum. Consultato: 18 febbraio 2025. [Online]. Disponibile su: https://www.weforum.org/stories/2024/11/the-role-of-energy-storage-technologies-in-the-energy-transition/

[29] V. Dias, M. Pochet, F. Contino, e H. Jeanmart, «Energy and Economic Costs of Chemical Storage», *Front. Mech. Eng.*, vol. 6, mag. 2020, doi: 10.3389/fmech.2020.00021.

[30] «Ammonia's Role in a Net-Zero Hydrogen Economy», Kleinman Center for Energy Policy. Consultato: 22 febbraio 2025. [Online]. Disponibile su: https://kleinmanenergy.upenn.edu/research/publications/ammonias-role-in-a-net-zero-hydrogen-economy/

[31] E. Spatolisano, L. A. Pellegrini, A. R. de Angelis, S. Cattaneo, e E. Roccaro, «Ammonia as a Carbon-Free Energy Carrier: NH3 Cracking to H2», *Ind. Eng. Chem. Res.*, vol. 62, fasc. 28, pp. 10813–10827, lug. 2023, doi: 10.1021/acs.iecr.3c01419.

[32] S. Garcia-Segura, M. Lanzarini-Lopes, K. Hristovski, e P. Westerhoff, «Electrocatalytic reduction of nitrate: Fundamentals to full-scale water

treatment applications», *Applied Catalysis B: Environmental*, vol. 236, pp. 546–568, nov. 2018, doi: 10.1016/j.apcatb.2018.05.041.

[33] D. M. Weekes, D. A. Salvatore, A. Reyes, A. Huang, e C. P. Berlinguette, «Electrolytic CO2 Reduction in a Flow Cell», *Acc. Chem. Res.*, vol. 51, fasc. 4, pp. 910–918, apr. 2018, doi: 10.1021/acs.accounts.8b00010.

[34] «(PDF) Electrochemical nitrogen reduction to ammonia using mesoporous iron oxide with abundant oxygen vacancies», *ResearchGate*, dic. 2024, doi: 10.1039/D3SE00369H.

[35] H. Y. Cha, Y. Park, K.-W. Seong, e K. Y. Park, «Electrochemical reduction of nitrate using divided electrolytic cell by proton exchange membrane», *1*, vol. 12, fasc. 4, Art. fasc. 4, lug. 2021.

[36] M. Leonardi, G. Tranchida, R. Corso, R. G. Milazzo, S. A. Lombardo, e S. M. S. Privitera, «Role of the Membrane Transport Mechanism in Electrochemical Nitrogen Reduction Experiments», *Membranes*, vol. 12, fasc. 10, Art. fasc. 10, ott. 2022, doi: 10.3390/membranes12100969.

[37] N. Pirrone, S. Garcia-Ballesteros, S. Hernández, e F. Bella, «Membrane/electrolyte interplay on ammonia motion inside a flow-cell for electrochemical nitrogen and nitrate reduction», *Electrochimica Acta*, vol. 493, p. 144415, lug. 2024, doi: 10.1016/j.electacta.2024.144415.

[38] «Nafion™ perfluorinated membrane Nafion™ 117, thickness 0.007 in., sheet size 7.5 cm × 13.0 cm | 31175-20-9». Consultato: 4 febbraio 2025. [Online]. Disponibile su: https://www.sigmaaldrich.com/IT/it/product/aldrich/915270

[39] S. S. Gadegaonkar, Ü. Mander, e M. Espenberg, «A state-of-the-art review and guidelines for enhancing nitrate removal in bio-electrochemical systems (BES)», *Journal of Water Process Engineering*, vol. 53, p. 103788, lug. 2023, doi: 10.1016/j.jwpe.2023.103788.

[40] Y. Wang e J. Qu, «Electrocatalytic Reduction of Nitrate in Water with a Palladium-Modified Copper Electrode», *Water Environment Research*, vol. 78, fasc. 7, pp. 724–729, 2006, doi: 10.2175/106143006X110665.

[41] «23.1: Reference Electrodes», Chemistry LibreTexts. Consultato: 25 febbraio 2025. [Online]. Disponibile su: https://chem.libretexts.org/Bookshelves/Analytical_Chemistry/Instrumental_Analysis_(LibreTexts)/23%3A_Potentiometry/23.01%3A_Reference_Electrodes

[42] «Frost Diagram». Consultato: 3 marzo 2025. [Online]. Disponibile su: https://encyclopedia.pub/entry/37475

[43] I. Katsounaros e G. Kyriacou, «Influence of the concentration and the nature of the supporting electrolyte on the electrochemical reduction of nitrate on tin cathode», *Electrochimica Acta*, vol. 52, fasc. 23, pp. 6412–6420, lug. 2007, doi: 10.1016/j.electacta.2007.04.050.

[44] Y. Wang, C. Wang, M. Li, Y. Yu, e B. Zhang, «Nitrate electroreduction: mechanism insight, in situ characterization, performance evaluation, and challenges», *Chem. Soc. Rev.*, vol. 50, fasc. 12, pp. 6720–6733, giu. 2021, doi: 10.1039/D1CS00116G.

[45] D. Anastasiadou, Y. van Beek, E. J. M. Hensen, e M. Costa Figueiredo, «Ammonia electrocatalytic synthesis from nitrate», *Electrochemical Science Advances*, vol. 3, fasc. 5, p. e2100220, 2023, doi: 10.1002/elsa.202100220.

[46] G. Horányi e E. M. Rizmayer, «Role of adsorption phenomena in the electrocatalytic reduction of nitric acid at a platinized platinum electrode», *Journal of Electroanalytical Chemistry and Interfacial Electrochemistry*, vol. 140, fasc. 2, pp. 347–366, nov. 1982, doi: 10.1016/0022-0728(82)85178-4.

[47] T. Hu, C. Wang, M. Wang, C. M. Li, e C. Guo, «Theoretical Insights into Superior Nitrate Reduction to Ammonia Performance of Copper Catalysts», *ACS Catal.*, vol. 11, fasc. 23, pp. 14417–14427, dic. 2021, doi: 10.1021/acscatal.1c03666.

[48] F. Yao *et al.*, «Indirect electrochemical reduction of nitrate in water using zero-valent titanium anode: Factors, kinetics, and mechanism», *Water Research*, vol. 157, pp. 191–200, giu. 2019, doi: 10.1016/j.watres.2019.03.078.

[49] «In Situ/Operando Methods for Understanding Electrocatalytic Nitrate Reduction Reaction | Request PDF», *ResearchGate*, dic. 2024, doi: 10.1002/smtd.202300169.

[50] H. Zhang, C. Wang, H. Luo, J. Chen, M. Kuang, e J. Yang, «Iron Nanoparticles Protected by Chainmail-structured Graphene for Durable Electrocatalytic Nitrate Reduction to Nitrogen», *Angewandte Chemie International Edition*, vol. 62, fasc. 5, p. e202217071, 2023, doi: 10.1002/anie.202217071.

[51] J. Ding, W. Li, Q.-L. Zhao, K. Wang, Z. Zheng, e Y.-Z. Gao, «Electroreduction of nitrate in water: Role of cathode and cell configuration», *Chemical Engineering Journal*, vol. 271, pp. 252–259, lug. 2015, doi: 10.1016/j.cej.2015.03.001.

[52] «In Situ Reconstruction of Partially Hydroxylated Porous Rh Metallene for Ethylene Glycol-Assisted Seawater Splitting - Mao - 2022 - Advanced Functional Materials - Wiley Online Library». Consultato: 6 marzo 2025. [Online]. Disponibile su: https://advanced.onlinelibrary.wiley.com/doi/abs/10.1002/adfm.202201081?casa_token=qrdsZxBZIkAAAAAA%3A-A-qyu7RWicsZq17YH9dYF192ybM-u842Ij_q5nHCgZwuWLtjT-SFi3lMXVVfvA2LBfBoyl71D5N5t0

[53] «Toray Carbon Paper 060, Wet Proofed». Consultato: 28 gennaio 2025. [Online]. Disponibile su: https://www.fuelcellstore.com/toray-carbon-paper-060

[54] A. Atrashkevich, A. S. Fajardo, P. Westerhoff, W. S. Walker, C. M. Sánchez-Sánchez, e S. Garcia-Segura, «Overcoming barriers for nitrate electrochemical reduction: By-passing water hardness», *Water Research*, vol. 225, p. 119118, ott. 2022, doi: 10.1016/j.watres.2022.119118.

[55] R. Cardeña, B. Cercado, e G. Buitrón, «Chapter 7 - Microbial Electrolysis Cell for Biohydrogen Production», in *Biohydrogen (Second Edition)*, A. Pandey, S. V. Mohan, J.-S. Chang, P. C. Hallenbeck, e C. Larroche, A c. di, in

Biomass, Biofuels, Biochemicals. , Elsevier, 2019, pp. 159–185. doi: 10.1016/B978-0-444-64203-5.00007-1.

[56] J. J. Giner-Sanz, G. Leverick, V. Pérez-Herranz, e Y. Shao-Horn, «Optimization of the salicylate method for ammonia quantification from nitrogen electroreduction», *Journal of Electroanalytical Chemistry*, vol. 896, p. 115250, set. 2021, doi: 10.1016/j.jelechem.2021.115250.

[57] H. Verdouw, C. J. A. Van Echteld, e E. M. J. Dekkers, «Ammonia determination based on indophenol formation with sodium salicylate», *Water Research*, vol. 12, fasc. 6, pp. 399–402, gen. 1978, doi: 10.1016/0043-1354(78)90107-0.

[58] «Ammonia-API colorimetric assay», IO Rodeo Blog. Consultato: 1 febbraio 2025. [Online]. Disponibile su: https://blog.iorodeo.com/ammonia-api-colorimetric-assay/

[59] Y. Bai *et al.*, «FCF-LDH/BiVO4 with synergistic effect of physical enrichment and chemical adsorption for efficient reduction of nitrate», *Green Energy & Environment*, vol. 9, fasc. 7, pp. 1112–1121, lug. 2024, doi: 10.1016/j.gee.2023.05.011.

[60] M. J. Moorcroft, J. Davis, e R. G. Compton, «Detection and determination of nitrate and nitrite: a review», *Talanta*, vol. 54, fasc. 5, pp. 785–803, giu. 2001, doi: 10.1016/S0039-9140(01)00323-X.